# Isolation of $[Ru(IPr)_2(CO)H]^+$ (IPr = 1,3-bis(2,6-diisopropylphenyl)-imidazol-2-ylidene) and reactivity towards E-H (E = H, B) bonds

Ian M. Riddlestone,[†] David McKay,[‡,δ] Matthias J. Gutmann,[$] Stuart A. Macgregor,[*,‡] Mary F. Mahon,[*,†] Hazel A. Sparkes[*,§] and Michael K. Whittlesey[*,†]

[†]Department of Chemistry, University of Bath, Claverton Down, Bath BA2 7AY, UK

[‡]Institute of Chemical Sciences, Heriot-Watt University, Edinburgh EH14 4AS, UK

[$]ISIS Facility, STFC-Rutherford Appleton Laboratory, Didcot OX11 OQX, UK

[§]School of Chemistry, University of Bristol, Cantock's Close, Bristol BS8 1TS, UK

*Supporting Information Placeholder*

**ABSTRACT:** Halide abstraction from the ruthenium N-heterocyclic carbene complex $Ru(IPr)_2(CO)HCl$ (**1**: IPr = 1,3-bis(2,6-diisopropylphenyl)imidazol-2-ylidene) with $NaBAr_4^F$ ($BAr_4^F$ = $B\{C_6H_3(3,5\text{-}CF_3)_2\}_4$) gave the salt $[Ru(IPr)_2(CO)H]BAr_4^F$ (**2**), which was shown through a combined X-ray/neutron structure refinement and Quantum Theory of Atoms in Molecules (QTAIM) study to contain a bifurcated Ru···η³-$H_2C$ ξ-agostic interaction involving one iPr substituent of the IPr ligand. This system complements the previously reported $[Ru(IMes)_2(CO)H]^+$ cation (IMes = 1,3-bis(2,4,6-trimethylphenyl)imidazol-2-ylidene: *Organometallics* **2009**, *28*, 1758) where a non-agostic form is favored. Treatment of **2** with CO, $H_2$ and the amine-boranes $H_3B{\cdot}NR_2H$ (R = Me, H) gave the coordinatively saturated products $[Ru(IPr)_2(CO)_3H]BAr_4^F$ (**3**), $[Ru(IPr)_2(CO)(\eta^2\text{-}H_2)H]BAr_4^F$ (**4**) and $[Ru(IPr)_2(CO)(\kappa^2\text{-}H_2BH{\cdot}NR_2H)H]BAr_4^F$ (R = Me, **5**, R = H, **6**) respectively. Heating **5** in the presence of $Me_3SiCH{=}CH_2$ led to alkene hydroboration and formation of the C-H activated product $[Ru(IPr)(IPr')(CO)]BAr_4^F$ (**7**). X-ray characterization of **3** and **5**-**7** was complemented by DFT calculations and the mechanism of H2/H exchange in **4** was also elucidated. Treatment of **2** with HBcat resulted in Ru-H abstraction to form the boryl complex $[Ru(IPr)_2(CO)(Bcat)]BAr_4^F$ (**8**), which proved to be competent in the catalytic hydroboration of 1-hexene. In **8**, a combined X-ray/neutron structure refinement and QTAIM analysis suggested the presence of a single Ru···η²-HC ξ-agostic interaction.

## INTRODUCTION

The preparation of coordinatively unsaturated transition metal complexes is a widespread pursuit for practitioners of organometallic chemistry with an eye to developing new or improved reactivity of organic substrates. In the case of ruthenium, efforts to generate low-coordinate Ru(0) species date from the mid 1960's with Chatt's attempted synthesis of the 16-electron chelating phosphine complex $Ru(dmpe)_2$ (dmpe = 1,2-bis(dimethylphosphino)ethane),[1] which was employed in some of the earliest attempts to bring about intra- and intermolecular C-H bond activation.[2] It is now known that this species is far too reactive to exist as anything other than a transient intermediate that can only be detected at very low temperature in inert gas matrices or in solution on very short, pico- to nanosecond timescales.[3] However, some 30 years after Chatt's studies, Caulton[4] and Werner[5] demonstrated that $Ru(0)L_4$ species could indeed be isolated (and even structurally characterized) given the appropriate choice of L ligands, namely bulky phosphines in combination with π-accepting carbonyl or nitrosyl groups.

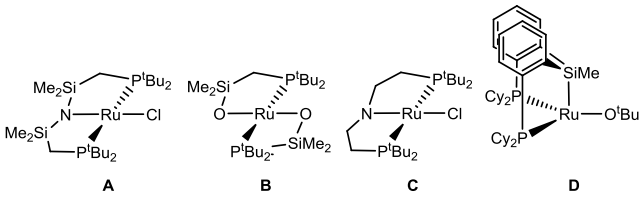


**Chart 1**

Arguably, the preparation of four-coordinate $Ru(II)L_4$ species is an even greater synthetic challenge on the grounds of their greater electron deficiency i.e. 14-electron count. Such species are therefore, unsurprisingly, rare (Chart 1). The chelate complexes Ru(PNP)Cl (**A**) and $Ru(PO)_2$ (**B**) adopt triplet ground states, which appear to be enough to reduce their Lewis acid character.[6] Upon changing $N(SiMe_2CH_2P^tBu_2)_2$ for $N(CH_2CH_2P^tBu_2)_2$,

Ru(PNP)Cl (**C**) displays a square planar structure and a singlet ground state due to the combination of high ligand sterics and strong N→Ru π-donation.[7] This same combination of steric and electronic donor properties also appears to help rationalize the stability of (Cy-PSiP)RuO$^t$Bu (**D**).[8]

In other species, such as [Ru($P^tBu_2Me$)$_2$(CO)R]$^+$ (R = Ph, H)[9-11] and Ru($PPh_2${2,6-$C_6Me_2H_3$})$_2Cl_2$ (Chart 2),[12] stabilization benefits from the presence of Ru···H-C agostic interactions to afford complexes which react as latent 14-electron species.[12-15] Thus, the X-ray structures of both [Ru($P^tBu_2Me$)$_2$(CO)Ph]$^+$ and [Ru($P^tBu_2Me$)$_2$(CO)H]$^+$ exhibit sawhorse configurations, in which both of the remaining vacant coordination sites at ruthenium are occupied by agostic interactions from the phosphine $^t$Bu groups. In the case of Ru($PPh_2${2,6-$C_6Me_2H_3$})$_2Cl_2$, neutron diffraction reveals an even more unusual stabilizing effect involving two sets of bifurcated (or dihapto) agostic Ru···η$^3$-$H_2C$ interactions.[16]

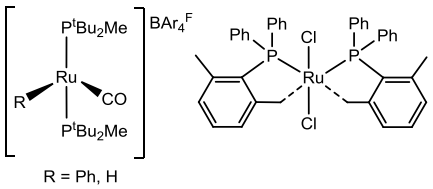


**Chart 2**

Our interest in Ru(II)$L_4$ species was raised by the report of Gunnoe and co-workers from a number of years ago which identified the cationic N-heterocyclic carbene (NHC) derivative, [Ru(IMes)$_2$(CO)H]$^+$ (**1**, Scheme 1: IMes = 1,3-bis(2,4,6-trimethylphenyl)imidazol-2-ylidene) as a true, four-coordinate Ru(II) species devoid of any agostic stabilisation.[17] All attempts to isolate **1** for structural verification proved, unfortunately, unsuccessful, and hence characterization was based upon DFT calculations and chemical trapping experiments. Given that variation of NHC N-substituents can be used to bring about often very subtle changes in the structure/reactivity of coordinatively unsaturated M(NHC)$_x$ complexes,[18] we have employed the bulkier IPr (1,3-bis(2,6-diisopropylphenyl)imidazol-2-ylidene) ligand for the generation of [Ru(IPr)$_2$(CO)H]$^+$ (**2**). Structural methods (neutron/X-ray diffraction) and DFT calculations have shown that **2** is stabilized by a symmetric bifurcated Ru···η$^3$-$H_2C$ ξ-agostic interaction involving an $^i$Pr methyl group. In solution, **2** undergoes facile coordination of neutral donor ligands (CO, $H_3B{\cdot}NR_2H$ (R = Me, H)), B-H activation of a borane as well as intramolecular C-H activation of an IPr ligand.

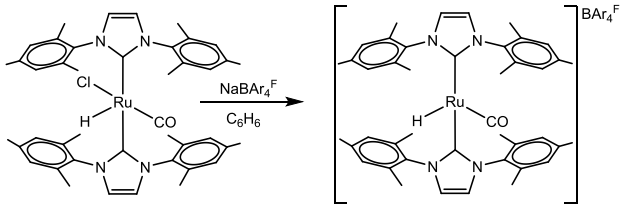


**Scheme 1** Gunnoe's reported synthesis of [Ru(IMes)2(CO)H]$BAr_4^F$ (**1**).[17]

## RESULTS AND DISCUSSION

**Synthesis and Characterization of [Ru(IPr)$_2$(CO)H]$^+$.** The $BAr_4^F$ (B{$C_6H_3$(3,5-$(CF_3)_2$}$_4$) salt of [Ru(IPr)$_2$(CO)H]$^+$ (**2**) was isolated in high yield (80%) as a highly air- and moisture-sensitive dark orange solid upon chloride abstraction from Ru(IPr)$_2$(CO)HCl[19] with $NaBAr^F{}_4$ in $C_6H_5F$ at room temperature over 12 h (Scheme 2).

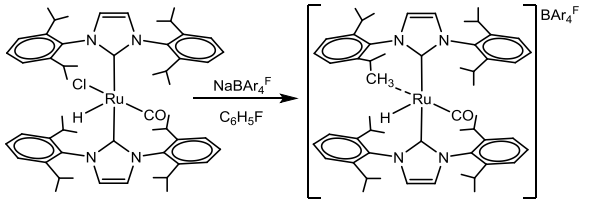


**Scheme 2** Synthesis of the $BAr_4^F$ salt of [Ru(IPr)$_2$(CO)H]$^+$ (**2**). Both here and in later figures, the dotted contact between Ru and an $^i$Pr methyl group represents the likelihood that some H3C···Ru agostic interaction is retained in solution.

An X-ray structure determination on crystals of the compound isolated from fluorobenzene/hexane revealed two components, which in each case, showed the presence of an ξ-agostic interaction between the metal and one of the $^i$Pr methyl substituents. This agostic C-H interaction lies *trans* to the CO group, with the hydride ligand disordered over two sites. To examine this in more detail, neutron diffraction data were combined with those from the X-ray measurement in a joint refinement. The cation of the major (55%) component (**2a**) is shown in Figure 1. Interestingly, the presence of two similar, short Ru···H-C contacts (Ru(1)···H(51A) 2.21(2) Å, Ru(1)···H(51B) 2.14(2) Å) supported the presence of a bifurcated Ru···η$^3$-$H_2C$ agostic interaction far more symmetric in nature than that seen in Ru($PPh_2${2,6-$C_6Me_2H_3$})$_2Cl_2$, where the Ru···H-C distances ranged from 2.113(10)-2.507(11) Å.[16] Conejero has reported that the C-H activated NHC complex [Pt(IPr)(IPr)′]$SbF_6$[20] exhibits a single ξ-agostic interaction to the non-activated IPr ligand with Pt···H and Pt···C distances of 2.017(6) and 2.8760(1) Å respectively, and Pt···H-C angle of 145°. In **2a**, the Ru(1)···C(51) distance is considerably shorter (2.589(3) Å), with Ru···H-C angles (Ru(1)···H(51A)-C(51)/Ru(1)···H(51B)-C(51)) of 97.4(11) and 100.2(11)°.

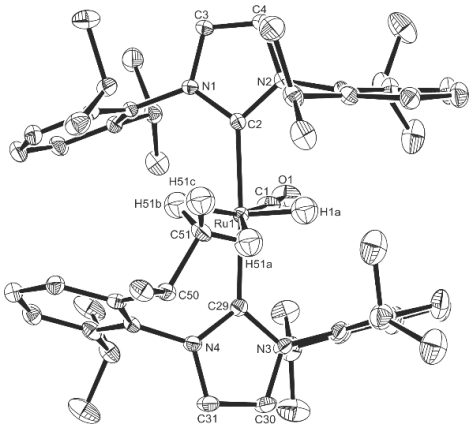


**Figure 1.** Combined neutron/X-ray structure of the cation in $[Ru(IPr)_2(CO)H]BAr_4^F$ (major component, **2a**). Ellipsoids are shown at the 30% level with all hydrogen atoms (except Ru-H and those on the agostic methyl group) removed for clarity. Selected bond lengths (Å) and angles (°): Ru(1)-C(2) 2.102(3), Ru(1)-C(29) 2.091(4), Ru(1)-C(1) 1.796(4), Ru(1)···C(51) 2.591, Ru(1)···H(51A) 2.21(2), Ru(1)···H(51B) 2.14(2), C(51)-H(51A) 1.09(2), C(51)-H(51B) 1.13(2), C(1)-O(1) 1.160(5), C(2)-Ru(1)-C(29) 176.51(13).

Further insight into the nature of the agostic interaction in **2a** was obtained from a Quantum Theory Atoms in Molecules (QTAIM)[21] study where the experimental structure of **2a** was used directly in the QTAIM analysis (Figure 2). This highlights curved bond paths associated with both the Ru···H51a and Ru1···H51b contacts, indicative of bonding interactions and so consistent with a bifurcated Ru···η³-$H_2C$ structure. This is further confirmed by the presence of a ring critical point (RCP) enclosed by the {Ru1···H51b-C51-H51a} unit. The computed BCP electron densities, $\rho(r)$, are relatively low at *ca*. 0.035 au, and suggest that, despite the short Ru···H51a/H51b and Ru···C51 distances, the resultant agostic interactions are relatively weak.[22]

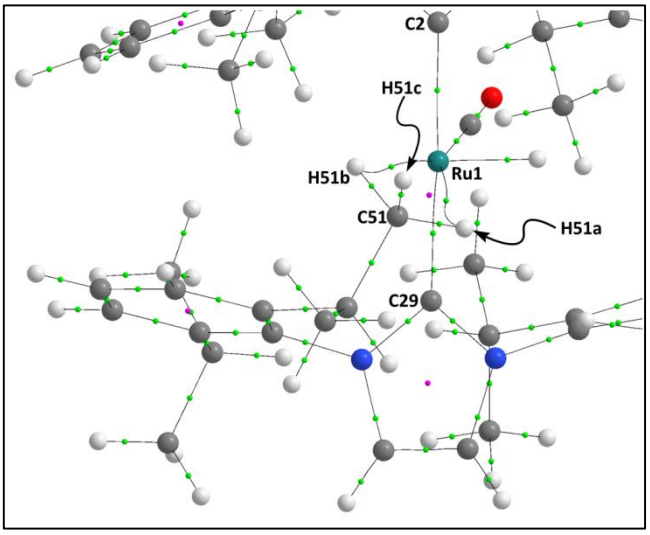


**Figure 2.** QTAIM molecular graph of the cation of the major component, **2a**, focusing on the Ru1···H51a/H51b interactions. Calculations were based on the experimental X-ray/neutron structure and used the BP86 functional. Bond critical points (BCPs) and ring critical points (RCPs) are shown as green and magenta spheres respectively. Selected $\rho(r)$ values (au): BCPs – Ru1···H51b 0.038; Ru1···H51a 0.033; RCP – Ru1···H51b-C51-H51a 0.033. See ESI for full AIM metrics.

**2b**, the cation within the second component present in the combined neutron/X-ray structure of **2**,[23] shows a very similar geometry around Ru1 to **2a**, with Ru···H51a and Ru1···H51b contacts of 2.23(2) Å and 2.16(2) Å respectively and a short Ru-C(51) contact of 2.590(3) Å. QTAIM calculations also confirm a bifurcated structure. In addition, a third Ru··· Ru···η²-HC contact of 2.44(2) Å to a iPr substituent located trans to the hydride ligand is seen, although the associated BCP has a low $\rho(r)$ value of only 0.012 au (see Computational ESI).

We were unable to affirm that the Ru···H-C interactions persisted in solution as the four doublets and two septets of the $^i$Pr groups observed by $^1$H NMR spectroscopy at room temperature simply broadened rather than separated upon cooling to 194 K.[24] Low temperature (200 K) $^{13}C\{^1H\}$ and $^1$H-coupled $^{13}$C NMR spectra showed neither any low frequency shifted methyl resonance nor any reduced $^1J_{CH}$ coupling constant (ESI). The low frequency of the hydride chemical shift (δ -23.9 at 298 K) was similar to that of both $Ru(IPr)_2(CO)HCl$ and **1** as a result of the vacant *trans* coordination site. Notably, NMR measurements of **2** (including overnight accumulated $^{13}$C spectra) could be recorded in $CD_2Cl_2$ and gave near identical spectra to those recorded in fluorobenzene, revealing that unlike $[Ru(P^tBu_2Me)_2(CO)H]^+$, there was no binding of dichloromethane.[11,25] Presumably, the Lewis acidity of **2** is lowered by the presence of the two strongly σ-donating NHC ligands which, in combination with their steric bulk, disfavor interaction with a poor base like $CH_2Cl_2$. A small amount of decomposition of **2** was evident by NMR spectroscopy (only after several days) in chlorinated solvents or upon warming to 343 K in $C_6H_5F$, although there was no evidence to suggest that this involved dehydrogenation of the carbene N-substituent as seen for $[Ir(IPr)_2H_2]^+$.[26]

**Experimental and Computational Comparison of $[Ru(IPr)_2(CO)H]^+$ and $[Ru(IMes)_2(CO)H]^+$.** In Gunnoe's attempts to prepare **1**, benzene was used as the solvent for the attempted $NaBAr_4^F$ abstraction. Upon turning to $C_6H_5F$, we found no discernible change in color of the solution, but did observe a change in the hydride region of the proton NMR spectrum, the signal for **1** at δ -25.4 being replaced by a new resonance at δ -29.9 within the time of mixing $Ru(IMes)_2(CO)HCl$ and $NaBAr_4^F$. The species responsible for this new signal proved to be stable for at least 48 h. Comparison with Aldridge's studies on $NaBAr_4^F$ abstraction of chloride from $M(IMes)_2H_2Cl$ (M = Rh, Ir),[26] in particular the shift of the hydride signal to lower frequency, led us to propose the formation of the sodium inclusion complex,

$[Ru(IMes)_2(CO)HCl(Na)]BAr_4^F$, in which the sodium cation is intercalated between the mesityl rings of the NHC. All efforts to isolate this species with the aim of confirming this assignment were unsuccessful. Similar behavior was found upon re-examining the $Ru(IPr)_2(CO)HCl/NaBAr_4^F$ reaction. A $^1H$ NMR spectrum recorded 15 min after mixing the reagents showed loss of the starting Ru-H resonance (δ -24.5) and formation of new signals at both higher (δ -23.9) and lower (δ -28.2) frequencies, assigned to **2** and $[Ru(IPr)_2(CO)HCl(Na)]BAr_4^F$ respectively. After 48 h, only the hydride signal for **2** remained, consistent with the inclusion complex being an intermediate on the pathway to full metathesis. Quite why the IMes derivative is so much longer lived than the IPr derivative is unclear. Different behavior was also apparent using $[Et_3Si(toluene)]BAr_4^F$ for halide abstraction instead of $NaBAr_4^F$. $Ru(IPr)_2(CO)HCl$ was now converted instantly and cleanly through to **2**, whereas with $Ru(IMes)_2(CO)HCl$, there was no clear evidence for the formation of a hydride-containing product at all.

As structural comparison of **1** and **2** was not possible experimentally, DFT calculations were employed to probe the differences between these two systems. Geometries were now fully optimized with the BP86 functional: for **2a** and **2b** input geometries were based on the X-ray/neutron structures, and these structures were adapted to produce input geometries for their IMes analogues **1a** and **1b**. The reported free energies include corrections for dispersion (D3 parameter set) and $C_6H_5F$ solution (PCM approach). For $[Ru(IPr)_2(CO)H]^+$, the optimized structures of **2a** and **2b** gave good agreement in the heavy atom positions, but saw rotation around the C(50)-C(51) bond such that the bifurcated Ru···η³-H2C agostic interactions are replaced by a single Ru···η²-H(51a)-C(51) agostic (**2a**: Ru(1)···H(51a) = 2.01 Å; Ru(1)···H(51b) = 2.54; **2b**: Ru(2)···H(51a) = 1.96 Å; Ru(2)···H(51b) = 2.63 Å). In addition, for **2b**, the short Ru···H contact trans to hydride noted experimentally shortens to 2.14 Å in the calculated structure, which therefore features two single Ru···η²-H-C agostic interactions, one trans to each of the CO and H ligands.. In the course of these studies an alternative conformer bereft of any agostic interaction (**2c**) was also located in which the closest Ru···H contact was 3.87 Å. Of these three forms, **2b** is computed to be the most stable in $C_6H_5F$ solution with **2a** and **2c** respectively 0.8 and 3.0 kcal/mol higher in energy.

Three equivalent structures were also located for $[Ru(IMes)_2(CO)H]^+$, but now the non-agostic form **1c** was most stable in $C_6H_5F$ solvent (*cf.* **1a** at +1.8 kcal/mol and **1b** at +2.1 kcal/mol). Although these computed differences are small, the tendency to form agostic interactions is clearly greater in $[Ru(IPr)_2(CO)H]^+$ compared to $[Ru(IMes)_2(CO)H]^+$.[27] This reflects the greater ability of the $^i$Pr substituents to interact with the Ru center without undue deformation of the NHC ligand. For example, in **2a** the angle between the plane of the central imidzol-2-ylidine ring and that of the aryl group of the 2,6-$^i Pr_2C_6H_3$ substituent engaged in the agostic interaction is 75.3°, whereas the equivalent angle with the mesityl substituent in **1a** is 55.8°.

Further evidence for **2** retaining an agostic interaction in solution comes from the different colors observed for solutions of **1** ('brick red')[17] and **2** (orange). TDDFT calculations (CAMB3LYP($C_6H_5F$)//BP86) indicate the lowest-lying absorption is dominated by a *d-d* transition between the HOMO and LUMO of the system, and show that this is blue-shifted in the presence of an agostic interaction (**1a**: 440 nm; **1b**: 432 nm; **1c**: 477 nm; **2a**: 399 nm; **2b**: 390 nm; **2c**: 486 nm). This reflects the interaction of the C-H bond with the $\{Ru(NHC)_2(CO)H\}^+$ fragment (NHC = IMes, IPr) in the agostic structures **1a/1b** and **2a/2b** which has the effect of destabilizing the LUMO. Orbital plots are provided in the ESI.

**Coordination of CO, $H_2$ and B-H bonds to $[Ru(IPr)_2(CO)H]^+$.** Addition of 1 atm CO to a fluorobenzene solution of **2** resulted in displacement of the agostic bonding and coordination of two additional CO ligands to yield the 18-electron tricarbonyl compound, $[Ru(IPr)_2(CO)_3H]BAr_4^F$ (**3**, Scheme 3). The presence of a high-frequency shifted (δ -6.81) hydride singlet was indicative of the coordinative saturation.[13a] Use of $^{13}CO$ led to signal enhancement of just the two lowest frequencies of the three $^{13}C\{^1H\}$ NMR carbonyl resonances at δ 173, 190 and 193, consistent with the initial Ru-CO group being inert to substitution. The *cis*-$^{13}C$ labelled CO ligands (Scheme 3) showed the expected small (4 Hz) $^2J_{CC}$ splitting. Both coupled to the Ru-H resonance, to generate a doublet of doublets signal, with $^2J_{HC}$ couplings of 26.1 (*trans*) and 6.7 Hz (*cis*).

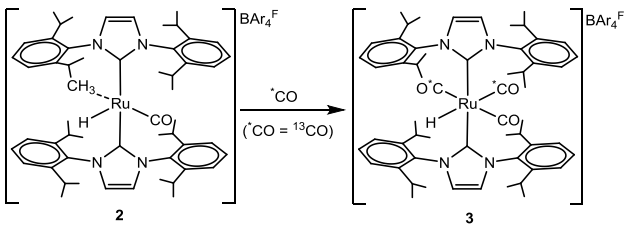


2 3

**Scheme 3**

Of note in the X-ray structure of **3** (Figure 3) were the distortions of the three distinctly non-linear Ru-C-O bonds. The 81° angle between the two mean planes (each containing the atoms of an NHC ring) revealed that the carbene ligands are disposed at the upper limit of a staggered arrangement. Moreover, the three carbonyl ligands about the equatorial girdle of the cation were each seen to lie atop an IMes phenyl ring (C55/O1 above ring based on C16; C56/O2 above ring based on C43 and C57/O3 above ring based on C31). The ensuing steric factors have combined such that the CO ligands are each bent away from the face of the aromatic ring above which each is located. These features are retained in the BP86-optimised structure of **3**, but lost in the less congested model species

$[Ru(IMe)_2(CO)_3H]^+$ (**3'**: IMe = 1,3-dimethylimidazol-2-ylidene) confirming their steric origin (similar deviations from linearity can also arise from electronic effects[4a]). The carbonyl oxygens appear to have borne the maximum brunt of these distortions as all three carbonyls exhibit acute Ru-C-O angles (Ru(1)-C(55)-O(1) 171.9(2)°, Ru(1)-C(56)-O(2) 171.6(2), Ru(1)-C(57)-O(3) 169.1(2)) away from the plane of the proximate aromatic ring. These compare to the values of 177.6(5), 176.9(5) and 175.1(5)° found in the cationic phosphine derivative $[Ru(PPh_3)_2(CO)_3H]^+$.[28] Ultimately, 'bowing' of the two *trans* carbonyl groups in **3** is evidenced by the C(56)-Ru(1)-C(57) angle of 166.09(12)°. The *trans*-influence of the hydride ligand manifests itself in the elongation of the Ru(1)-C(55) distance (1.976(3) Å) relative to the other two Ru-CO bond lengths (1.945(3) and 1.922(3) Å).

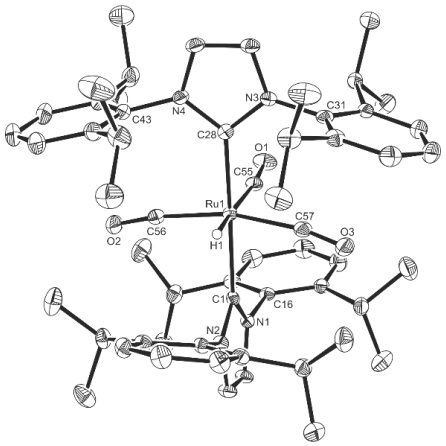


**Figure 3.** Molecular structure of the cation in $[Ru(IPr)_2(CO)_3H]BAr^F_4$ (**3**). Ellipsoids are shown at the 30% level with all hydrogen atoms (except Ru-H) removed for clarity. Selected bond lengths (Å) and angles (°): Ru(1)-C(1) 2.140(2), Ru(1)-C(28) 2.129(3), Ru(1)-C(55) 1.976(3), Ru(1)-C(56) 1.922(3), Ru(1)-C(57) 1.945(3), C(1)-Ru(1)-C(28) 171.64(10), C(55)-Ru(1)-C(56) 91.81(12), C(56)-Ru(1)-C(57) 166.09(12).

Introduction of $H_2$ (1 atm) into a $CD_2Cl_2$ solution of **2** brought about an immediate color change from orange to yellow resulting from the formation of the dihydrogen hydride complex $[Ru(IPr)_2(CO)(\eta^2\text{-}H_2)H]BAr^F_4$ (**4**, Scheme 4). At room temperature, this showed a single, broad hydride resonance at δ -4.95 of relative integral 3, suggestive of rapidly exchanging Ru-H/($\eta^2$-$H_2$) ligands. Even at 182 K, the exchange could not be frozen out, an observation that is in line with other ruthenium complexes containing a *cis*-arrangement of dihydrogen and hydride ligands.[29,30] Freeze-pump-thaw degassing failed to completely remove the $\eta^2$-$H_2$ ligand and the resonance at δ -4.95 could still be seen even after 10 degassing cycles.[31] Upon reducing the solution of **4** to complete dryness, **2** was regenerated.

DFT calculations were employed to provide structural insight into **4** and three local minima were again located, two of which feature a single agostic interaction, either trans to CO (**4a**) or H (**4b**), and a third, non-agostic form (**4c**). All three isomers are within 0.9 kcal/mol of each other when computed at the BP86-D3($CH_2Cl_2$) level (Figure 4(a)). A transition state for Ru-H/($\eta^2$-$H_2$) exchange, **TS(4b-4b)**, was also located. This process involves H-transfer from the original $\eta^2$-$H_2$ ligand in **4b** (labelled $H_a$-$H_b$, Figure 4(b)) onto the neighboring hydride ($H_c$). Concomitant rotation of this new $\eta^2$-$H_c$-$H_b$ moiety then delivers $H_c$ back onto $H_a$ to complete the exchange. In **TS(4b-4b)**, the agostic interaction shortens significantly (Ru···$H_d$ = 1.91 Å *cf.* 2.06 Å in **4b**) reflecting the lower trans influence of the $\eta^2$-$H_2$ moiety compared to a hydride. The overall barrier (relative to the lowest energy form **4c**) is 13.3 kcal/mol, consistent with rapid exchange on the NMR timescale.

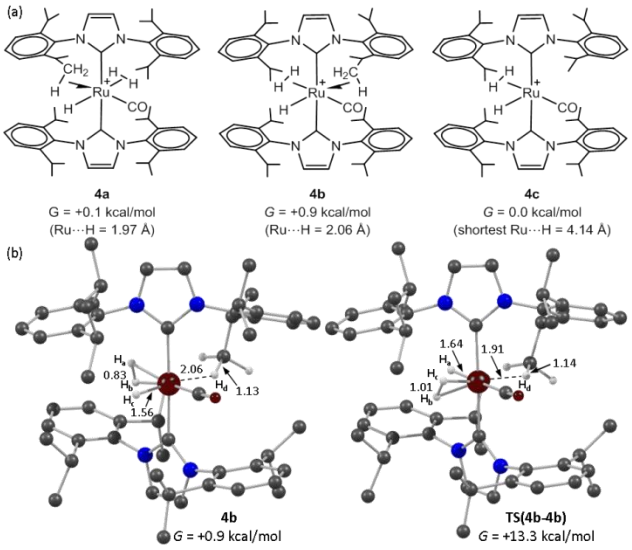


**Figure 4.** (a) Isomers of $[Ru(IPr)_2(CO)(\eta^2\text{-}H_2)H]^+$, **4**, with the shortest agostic Ru···H contact indicated; (b) Computed structures of **4b** and Ru-H/($\eta^2$-$H_2$) exchange transition state **TS(4b-4b)** with selected distances in Å; non-participating H atoms omitted for clarity. All free energies (kcal/mol) are at the BP86-D3($CH_2Cl_2$) level and are quoted relative to **4c** set to 0.0 kcal/mol.

The amine-borane complexes[32] $[Ru(IPr)_2(CO)(\kappa^2\text{-}H_2BH{\cdot}NMe_2H)H]BAr^F_4$ (**5**) and $[Ru(IPr)_2(CO)(\kappa^2\text{-}H_2BH{\cdot}NH_3)H]BAr^F_4$ (**6**) were prepared as alternative examples involving σ E-H bond coordination to **2** (Scheme 4). **5** and **6** were identified in the first instance by the appearance of $^{11}$B NMR signals at δ 4.5 and δ -2.4 respectively, characteristically downfield from those of the free substrates (δ -13.4, -21.6).[33,34] In the low frequency region of the $^1$H NMR spectra, sharp hydride signals (**5**: δ -15.61; **6**: δ -15.88) were present in a 1:3 ratio with very broad B-H resonances (**5**: δ -2.3; **6**: δ -2.1). Upon cooling to 190 K, exchange of the bound and terminal B-H groups was frozen out to give two distinct, single integral Ru-*H*-B singlets (**5**: δ -5.83, -3.94; **6**: δ -5.63, -4.13), which sharpened upon $^{11}$B decoupling. In the case of **5**, $^1$H{$^{11}$B} NOESY studies showed that the remaining, unbound B-H signal was hidden underneath resonances from the IPr groups

The X-ray structures of both **5** and **6** (Figure 5) revealed distorted octahedral geometries comprized of a *trans* arrangement of IPr ligands with the CO and hydride then mutually *cis* and, therefore, *trans* to the two metal bound B-H groups of the amine-borane ligands. The Ru···B distances of 2.293(4) and 2.333(2) Å were similar to the values in the large number of known rhodium κ²-bound derivatives (e.g. $[Rh(P^iBu_3)_2(\kappa^2\text{-}H_2BH{\cdot}NMe_2H)H_2]^+$ (2.318(8) Å),[33,35] $[Rh(IMes)_2(\kappa^2\text{-}H_2BH{\cdot}N^tBuH_2)H_2]^+$ (2.305(4) Å)[36]), although (unsurprisingly) significantly shorter than in the κ¹-bound ruthenium complexes, $[Ru(xantphos)(PPh_3)(\kappa^1\text{-}H_2BH{\cdot}NH_3)H]^+$ (2.939(3) Å)[37] and $[Cp'Ru(PMe_3)_2(\kappa^1\text{-}H_2BH{\cdot}NMe_3)]^+$ (2.648(3) Å).[38]

The stability of **5** in solution proved to be solvent dependent. Thus, the complex decomposed in $CD_2Cl_2$ over ca. 6 h at room temperature, but was stable for over a week in $C_6H_5F$. However, warming to 343 K in $C_6H_5F$ resulted in dehydrocoupling of the amine-borane ligand to afford $[Me_2N\text{-}BH_2]_2$ and the dihydrogen hydride complex **4**. Coordination of $H_2$ eliminated upon dehydrocoupling was also found[37] for $[Ru(xantphos)(PPh_3)(\kappa^1\text{-}H_2BH{\cdot}N^tBuH_2)H]^+$ whereas, in contrast, amino-borane products of the type $[ML_2(\kappa^2\text{-}H_2B\text{-}NR_2)H_2]^+$ arise upon the dehydrocoupling of Rh and Ir amine-borane derivatives.[39] This difference is not simply due to Ru vs Rh/Ir, since $Ru(PCy_3)_2(\eta^2\text{-}H_2)_2H_2$ has also been shown to form the amino-borane product $Ru(PCy_3)_2(\kappa^2\text{-}H_2B\text{-}NR_2)H_2$ upon direct addition of $H_3B{\cdot}NR_2H$ (R = H, Me).[40] Extension of the bonding analysis performed by Alcaraz *et al.* on the isoelectronic and isostructural complexes $[M(PCy_3)_2(\kappa^2\text{-}H_2B\text{-}N^iPr_2)H_2]^{n+}$ (M = Ru, n = 0; M = Rh and Ir, n = 1) suggests that the inability of cationic **2** to coordinate an amino-borane ligand

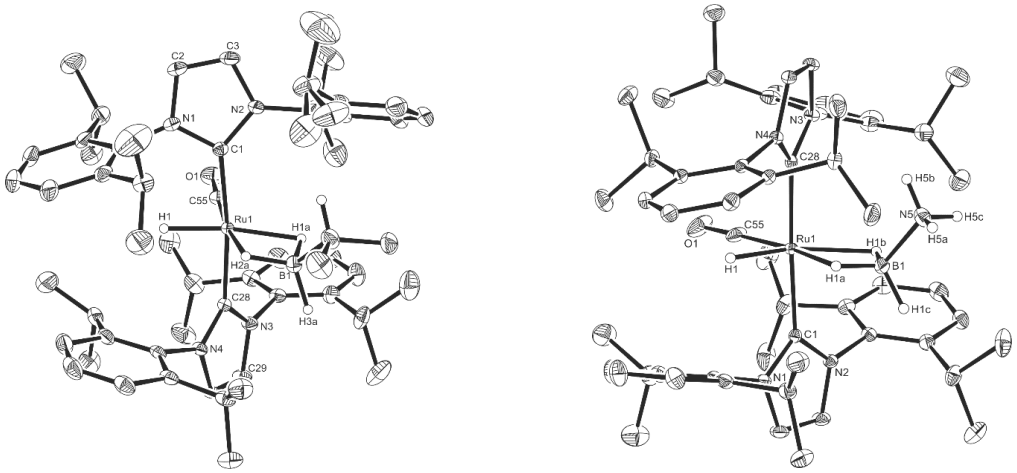


**Figure 5.** Molecular structure of the cations in (left) $[Ru(IPr)_2(CO)(\kappa^2\text{-}H_2BH{\cdot}NMe_2H)H]BAr^F_4$ (**5**) and (right) $[Ru(IPr)_2(CO)(\kappa^2\text{-}H_2BH{\cdot}NH_3)H]BAr^F_4$ (**6**). Ellipsoids are shown at the 30% level with all hydrogen atoms (except Ru-H and those on B or N) removed for clarity. Selected bond lengths (Å) and angles (°) in **5**: Ru(1)-C(1) 2.136(3), Ru(1)-C(28) 2.107(3), Ru(1)-C(55) 1.805(4), Ru(1)-B(1) 2.293(4), C(1)-Ru(1)-C(28) 173.11(13), C(55)-Ru(1)-B(1) 142.06(16). Selected bond lengths (Å) and angles (°) in **6**: Ru(1)-C(1) 2.1170(16), Ru(1)-C(28) 2.0950(16), Ru(1)-C(55) 1.813(2), Ru(1)-B(1) 2.333(2), C(1)-Ru(1)-C(28) 176.78(6), C(55)-Ru(1)-B(1) 162.34(10).

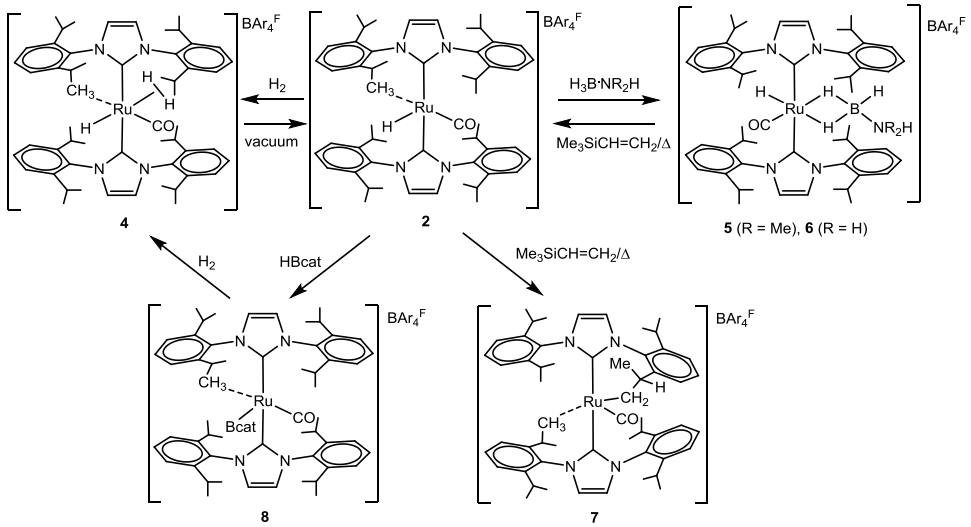


**Scheme 4**

may be connected to poor overlap between the contracted metal *d*-orbitals and empty BN $\pi^*$ orbital.[41]

In an attempt to promote $H_2B$-$NMe_2$ coordination, **5** was heated with an excess of $Me_3SiCH{=}CH_2$ as a hydrogen acceptor. This led, instead, to formation of the hydroboration product, $Me_3SiCH_2CH_2BH_2NMe_2H$, which was identified by comparison of the $^{11}$B NMR chemical shift to those of $RCH_2CH_2BH_2NMe_3$ (R = $^t$Bu, $Me(CH_2)_3$).[42] The initial organometallic product of the reaction was **2**, implying that alkene hydrogenation must occur as well as hydroboration. Continued heating led to the slow disappearance of the hydride signal for **2** (15 days at 323 K in $C_6H_5F$), alongside a change in color of the solution from orange to red. Spectroscopic identification of the product(s) proved to be a thankless task due to extensive overlap of signals in both the methyl and methine regions of the proton NMR spectrum.

Fortuitous isolation of a very small number of diffraction quality red-orange crystals proved possible. These were characterized by X-ray crystallography (Figure 6) as the C-H activated IPr complex, $[Ru(IPr)(IPr)'(CO)]BAr^F_4$ (**7**). The sawhorse structure (C(1)-Ru(1)-C(29): 175.67(9)°; C(28)-Ru(1)-C(12): 96.40(12)°) shows an agostic interaction *trans* to the activated arm of the IPr ligand (Ru(1)···H(51C) 2.23(2) Å, Ru(1)···C(51) 3.163(3) Å, Ru(1)-H(51C)-C(51) 158(2)°). This was confirmed by a QTAIM calculation based on the heavy atom positions of **7** that showed a Ru(1)···H51c bond path with $\rho(r)$ = 0.035 au (see Fig. S19, ESI). The metallated C-Ru distance of 2.071(2) Å is much shorter than in either $[Ir(IPr)'(IPr)''H]^+$ (2.117(7) Å)[43] or $[Pt(IPr)(IPr)']^+$ (2.226(6) Å)[20] which, to the best of our knowledge, are the only other known examples of C-H activated IPr complexes.

**B-H activation by 2**. The electrophilic nature of the Ru-H in **2** was demonstrated by the reaction with HBcat, which generated a rare example of a cationic boryl complex,[44] $[Ru(IPr)_2(CO)(Bcat)]BAr^F_4$ (**8**, Scheme 4). The formation of a boryl ligand was inferred in the first instance by a signal at ca. δ 42 in the $^{11}$B NMR spectrum, which is indicative of three-coordinate boron.[45] Free rotation about the Ru-B bond (based on the appearance of two proton and three $^{13}$C catechol signals) could be frozen out at 213 K, while lowering the temperature further (to 182 K) resolved the methine protons of the IPr ligands into eight multiplets, each of integral 1. The methyl resonances remained partially overlapping, although one doublet was low frequency shifted to δ -0.34, consistent with agostic bonding.

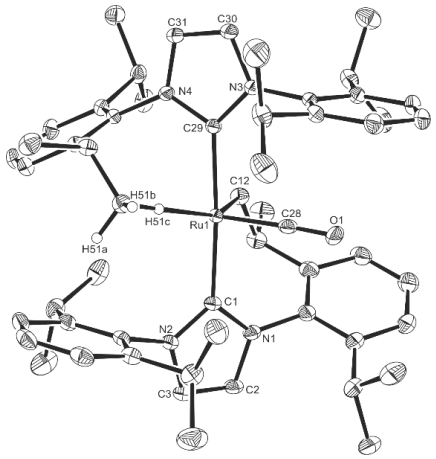


**Figure 6.** Molecular structure of the cation in $[Ru(IPr)(IPr)'(CO)]BAr^F_4$ (**7**). Ellipsoids are shown at the 30% level with all hydrogen atoms (except those on the agostic methyl group) removed for clarity. Selected bond lengths (Å) and angles (°): Ru(1)-C(1) 2.106(2), Ru(1)-C(29) 2.113(2), Ru(1)-C(28) 1.788(3), Ru(1)-C(12) 2.071(2), C(1)-Ru(1)-C(29) 175.67(9), C(12)-Ru(1)-C(28) 96.40(12).

This was investigated in the solid-state by a joint X-ray/neutron structure determination and QTAIM study. The former (Figure 7) revealed similar metrics to those seen in **2**, although with somewhat greater asymmetry in the closest Ru···H contacts (Ru(1)···C(27) 2.572 Å, Ru(1)···H(27b) 2.017 Å, Ru(1)···H(27) 2.463 Å, Ru(1)···H(27b)-C(27) 109.05°). The associated QTAIM molecular graph (Figure 8) this time indicates a single Ru···$\eta^2$-HC $^i$Pr ξ-agostic, with no bond path evident between Ru1 and H27a and, hence, no RCP that would be indicative of the bifurcated Ru···$\eta^3$-$H_2C$ form. The strong *trans*-influence boryl ligand[46,47] occupied the apical site of the square pyramidal structure, with much shorter Ru-B distance (2.030(4) Å) than found in other Ru or Os boryl complexes.[48] The catechol substituent provided the optimal motif for coordination to Ru, since no reaction at all was observed upon treatment of **2** with HBpin.

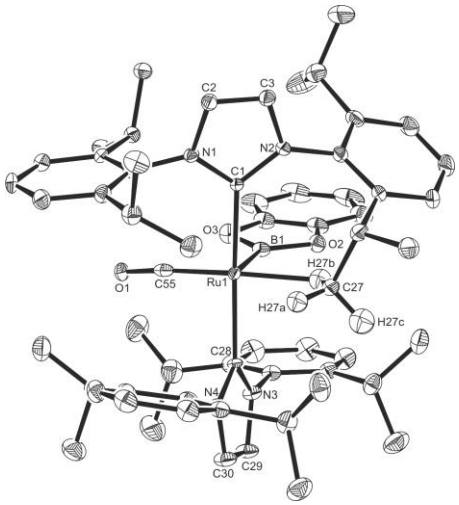


**Figure 7.** Combined X-ray/neutron structure of the cation in $[Ru(IPr)_2(CO)(Bcat)]BAr^F_4$ (**8**). Ellipsoids are shown at the

30% level with all hydrogen atoms (except those on the agostic methyl group) removed for clarity. Selected bond lengths (Å) and angles (°): Ru(1)-C(1) 2.141(4), Ru(1)-C(28) 2.138(4), Ru(1)-C(55) 1.834(5), Ru(1)-B(1) 2.030(4), C(1)-Ru(1)-C(28) 172.41(15), C(55)-Ru(1)-B(1) 84.1(2).

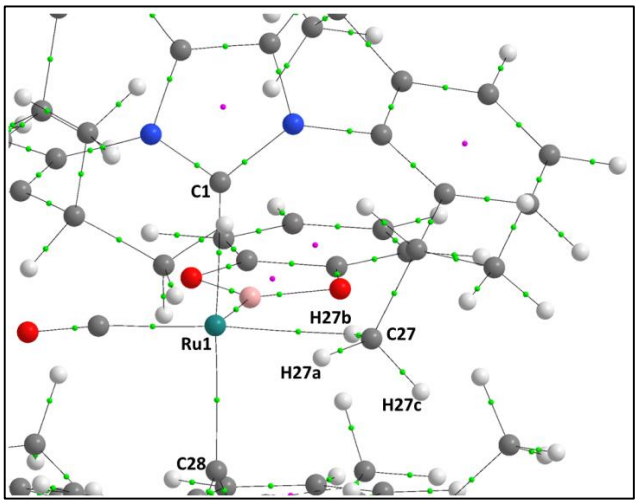


**Figure 8.** QTAIM molecular graph of **8** focusing on the Ru1···H27b interaction. Calculations were based on the experimental X-ray/neutron structure and used the BP86 functional. BCPs and RCPs are shown as green and magenta spheres respectively. $\rho(r)$ for the Ru1···H51b BCP = 0.042 au. See ESI for full QTAIM metrics.

The reasons why bifurcated Ru·····η³-$H_2C$ structures are seen in **2a** and **2b** while a Ru···η²-HC interaction is preferred in **8** are presently not clear to us. Our DFT calculations on the isolated cations of **2a** and **2b** indicate that structures with different (or indeed no) agostic interactions can be very close in energy. Moreover, a 2nd order perturbation analysis based on the computed natural bond orbitals (NBO) suggests the overall strength of the agostic interaction does not reflect the binding mode. Thus the total σ-donation from the C51-H51a and C51-H51b σ-BMOs is strongest in **2a** (21.2 kcal/mol), weakest in **2b** (12.4 kcal/mol), and intermediate from the C27-H27a and C27-H27b σ-BMOs in **8** (18.6 kcal/mol). See Figures S21 and S22 for full details.

**Catalytic hydroboration of alkenes with 8.** Upon exposure of **8** to 1 atm $H_2$, elimination of HBcat took place in the time of mixing with concomitant formation of the dihydrogen hydride complex **4**. The reversible coordination of the boryl ligand therefore prompted a preliminary study on the use of **8** as a precursor for catalytic alkene hydroboration. Rhodium, particularly with phosphine ligands,[49] is typically the element of choice for this transformation, with only a handful of reports detailing the activity of ruthenium complexes.[50] Catalytic experiments with 1-hexene showed that **8** gave mainly the linear hydroboration product, with a small amount of hexane also generated through competitive alkene hydrogenation (Table 1). The hydride complex **2** gave an identical product composition, suggesting that it is converted to **8** under the catalytic conditions, and that it is the boryl complex which then propagates the subsequent chemistry.[47]

**Table 1. Hydroboration of 1-hexene[a]**

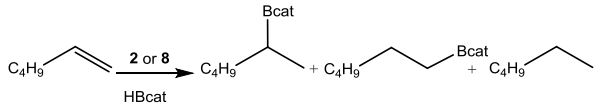


| Entry | Ru precursor | Product ratio[b] | | |
|---|---|---|---|---|
| | | Branched | Linear | Hexane |
| 1 | 8 | 14 | 80 | 6 |
| 2 | 2 | 18 | 76 | 6 |

[a]Conditions: 20 equiv alkene, 40 equiv HBcat in $C_6H_5F$, 298 K for 24 h, average of 2 runs. [b]Products and ratio determined by GC-MS and GC.

## SUMMARY AND CONCLUSIONS

The latent 4-coordinate Ru(II) complex $[Ru(IPr)_2(CO)H]BAr_4^F$ (**2**) has been prepared and shown by a combination of structural and computational methods to contain a bifurcated Ru···η³-$H_2C$ agostic interaction at one of the carbene $^i$Pr substituents. The agostic bonding appears to play a central role in allowing **2** to be isolated and structurally characterized, in contrast to the non-agostic IMes derivative. In terms of reactivity, **2** behaves like a coordinatively unsaturated fragment, readily coordinating $H_2$, CO and amine boranes. Treatment with catecholborane highlights the electrophilic nature of the Ru-H bond which results in the formation of the boryl derivative $[Ru(IPr)_2(CO)(Bcat)]BAr_4^F$, which features an Ru··· η²-HC interaction This mode of reactivity, whereby substrates E-H (E = B, H) can add over the Ru-H bond, appears to be especially promising as a route to new Ru-E containing products and is something we will report more on in due course.

## EXPERIMENTAL SECTION

All manipulations were carried out using standard Schlenk, high vacuum and glovebox techniques using dried and degassed solvents, unless otherwise stated. NMR spectra were recorded on Bruker Avance 400 and 500 MHz NMR spectrometers and referenced to residual solvent signals for $^1$H and $^{13}$C spectra for $C_6D_6$ (δ 7.15, 128.0) and $CD_2Cl_2$ (δ 5.32, 54.0). Unlocked samples in fluorobenzene were referenced to the center of the downfield multiplet at δ 7.11. $^{11}$B spectra were referenced externally to $BF_3{\cdot}OEt_2$ at δ = 0.0. All complexes, exhibited a singlet at δ -6.6 for the $BAr_4^F$ anion. IR spectra were recorded on a Nicolet Nexus spectrometer. Elemental analyses were performed by Elemental Microanalysis Ltd, Okehampton, Devon, UK. GC-MS data were collected on an Agilent Technologies 5975C using an HP-5 column (GC data was collected on the same type of column). $Ru(IPr)_2(CO)HCl$ was prepared according to the literature.[19]

**$[Ru(IPr)_2(CO)H]BAr_4^F$ (2).** A $C_6H_5F$ (8 mL) solution of $Ru(IPr)_2(CO)HCl$ (0.21 g, 0.21 mmol) was added to a slurry of $NaBAr_4^F$ (0.192 g, 0.22 mmol) in $C_6H_5F$ (2 mL) and the suspension stirred for 12 h. After filtration, the reaction mixture was concentrated to ca. 3 mL and layered with hexane to afford dark orange crystals of **2**, which were manually separated by hand

from colorless crystals of residual $NaBAr^F_4$. Yield: 0.290 g (80%). $^1$H NMR (500 MHz, $CD_2Cl_2$, 298 K): δ 7.74 (s, 8H, *o*-Ar-*H*), 7.58 (s, 4H, *p*-Ar-*H*), 7.45 (t, $^3J_{HH}$ = 7.7 Hz, 4H, *p*-Ar-*H*), 7.18-7.21 (overlapping d, 8H, *m*-Ar-*H*), 7.06 (s, 4H, NC*H*), 2.39 (sept, $^3J_{HH}$ = 7.0 Hz, 4H, C*H*($CH_3$)$_2$), 2.32 (sept, $^3J_{HH}$ = 6.8 Hz, 4H, C*H*($CH_3$)$_2$), 1.09 (d, $^3J_{HH}$ = 6.8 Hz, 12H, CH(C*H*$_3$)$_2$), 1.05 (d, $^3J_{HH}$ = 7.0 Hz, 12H, CH(C*H*$_3$)$_2$), 0.82 (d, $^3J_{HH}$ = 6.8 Hz, 12H, CH(C*H*$_3$)$_2$), 0.73 (d, $^3J_{HH}$ = 7.0 Hz, 12H, CH(C*H*$_3$)$_2$), -23.69 (s, 1H, Ru-*H*). $^{13}$C{$^1$H} NMR (126 MHz, $CD_2Cl_2$, 298 K): δ 200.2 (s, Ru-*C*O), 185.4 (s, Ru-$C_{NHC}$), 162.2 (q, $^1J_{CB}$ = 50 Hz, *i*-Ar*C*), 145.8 (s, *o*-Ar*C*), 145.7 (s, *o*-Ar*C*), 135.3 (s, *o*-Ar*C*), 135.2 (s, NAr*C*), 131.1 (s, *p*-Ar*C*), 129.4 (qq, $^2J_{CF}$ = 32.2 Hz, $^4J_{CF}$ = 3.1 Hz), *m*-Ar*C*), 125.8 (s, N*C*H), 125.1 (q, $^1J_{CF}$ = 270 Hz, *C*F$_3$), 125.0 (s, *m*-Ar*C*), 124.7 (s, *m*-Ar*C*) , 117.9 (sept, $^3J_{CF}$ = 4 Hz, *p*-Ar*C*), 29.2 (s, *C*H($CH_3$)$_2$), 29.2 (s, *C*H($CH_3$)$_2$), 24.6 (s, CH(*C*H$_3$)$_2$), 24.4 (s, CH(*C*H$_3$)$_2$), 23.8 (s, CH(*C*H$_3$)$_2$), 22.3 (s, CH(*C*H$_3$)$_2$). IR ($CH_2Cl_2$, cm$^{-1}$): 1964 ($\nu_{CO}$). Anal. Calcd for $C_{87}H_{85}BN_4OF_{24}Ru$: C 59.02, H 4.84, N 3.16. Found: C 58.91, H 5.00, N 3.29.

**[Ru(IPr)$_2$(CO)$_3$H]BAr$^F_4$ (3).** A J Young's resealable NMR tube was charged with a solution of **2** (0.043 g, 0.025 mmol) in $C_6H_5F$ (0.5 mL), degassed via three freeze-pump-thaw cycles and exposed to 1 atm CO. After 3 h, the pale yellow solution was layered with hexane to afford pale yellow crystals of **3**. Yield: 0.016 g (36%). $^1$H NMR (500 MHz, $CD_2Cl_2$, 298 K): δ 7.73 (s, 8H, *o*-Ar*H*), 7.56 (s, 4H, *p*-Ar*H*), 7.51 (t, $^3J_{HH}$ = 8.1 Hz, 4H, *p*-Ar*H*), 7.28 (d, $^3J_{HH}$ = 8.1 Hz, 8H, *m*-Ar*H*), 7.16 (s, 4H, NC*H*), 2.21 (sept, $^3J_{HH}$ = 7.0 Hz, 8H, C*H*($CH_3$)$_2$), 1.09 (d, $^3J_{HH}$ = 7.0 Hz, 24H, CH(C*H*$_3$)$_2$), 1.01 (d, $^3J_{HH}$ = 7.0 Hz, 24H, CH(C*H*$_3$)$_2$), -6.81 (s, 1H, Ru*H*). $^{13}$C{$^1$H} NMR (126 MHz, $CD_2Cl_2$, 298 K): δ 193.1 (s, Ru-*C*O), 189.6 (s, Ru-*C*O), 173.1 (s, Ru-$C_{NHC}$), 162.1 (q, $^1J_{CB}$ = 51 Hz, *i*-Ar*C*), 146.4 (s, *o*-Ar*C*), 136.6 (s, NAr*C*), 135.2 (s, *o*-Ar*C*), 132.0 (s, *p*-Ar*C*), 129.2 (qq, $^2J_{CF}$ = 32 Hz, $^4J_{CF}$ = 3 Hz, *m*-Ar*C*), 126.8 (s, N*C*H), 125.1 (s, *m*-Ar*C*), 125.0 (q, $^1J_{CF}$ = 271.1 Hz, *C*F$_3$), 117.8 (m, *p*-Ar*C*), 29.1 (s, *C*H($CH_3$)$_2$), 26.3 (s, CH(*C*H$_3$)$_2$), 22.6 (s, CH(*C*H$_3$)$_2$). IR (KBr, cm$^{-1}$): 2040 ($\nu_{CO}$), 2025 ($\nu_{CO}$). Anal. Calcd for $C_{87}{}^{13}C_2H_{85}BN_4O_3F_{24}Ru$: C 58.56, H 4.69, N 3.06. Found: C 58.39, H 4.60, N 3.00.

**[Ru(IPr)$_2$(CO)(η$^2$-H$_2$)H]BAr$^F_4$ (4)**. A J Young's resealable NMR tube was charged with a solution of **2** (0.010 g, 0.005 mmol) in $CD_2Cl_2$ (0.5 mL), degassed via three freeze-pump-thaw cycles and exposed to 1 atm $H_2$. After shaking the tube was then placed into the NMR spectrometer for characterization. $^1$H NMR (400 MHz, $CD_2Cl_2$, 182 K): δ 7.72 (s, 8H, *o*-Ar*H*), 7.53 (s, 4H, *p*-Ar*H*), 7.44 (t, $^3J_{HH}$ = 7.5 Hz, 4H, *p*-Ar*H*), 7.14 (d, $^3J_{HH}$ = 7.5 Hz 8H, *m*-Ar*H*), 7.11 (s, 4H, NC*H*), 1.95 (m, 8H, C*H*($CH_3$)$_2$), 0.89 (d, $^3J_{HH}$ = 5.4 Hz, 24H, CH(C*H*$_3$)$_2$), 0.82 (d, $^3J_{HH}$ = 5.4 Hz, 24H, CH(C*H*$_3$)$_2$), -4.95 (br s, 3H, Ru*H* + Ru(η$^2$-*H*$_2$)).

**[Ru(IPr)$_2$(CO)(κ$^2$-H$_2$BH·NMe$_2$H)H]BAr$^F_4$ (5).** $H_3B{\cdot}NMe_2H$ (6 μL of 1.7 M solution in $C_6H_5F$, 0.01 mmol) was added to a solution of **2** (0.019 g, 0.01 mmol) in $C_6H_5F$ (0.5 mL). After 2 h, the solvent was removed in vacuo, the residue was washed with hexane (3 x 0.4 mL) and then dried under vacuum. Layering the residue in fluorobenzene/hexane afforded pale yellow crystals of **5**. Yield: 0.017 g (78%). $^1$H NMR (400 MHz, $CD_2Cl_2$, 298 K): δ 7.74 (s, 8H, *o*-Ar*H*), 7.57 (s, 4H, *p*-Ar*H*), 7.48 (t, $^3J_{HH}$ = 7.8 Hz, 4H, Ar*H*), 7.23 (d, $^3J_{HH}$ = 7.8 Hz, 4H, Ar*H*), 7.20 (d, $^3J_{HH}$ = 7.8 Hz, 4H, Ar*H*), 7.00 (s, 4H, NC*H*), 2.75 (br s, 5H, N*H* + C*H*($CH_3$)$_2$), 2.50 (br s, 4H, C*H*($CH_3$)$_2$), 2.03/2.02 (s, 6H, N(C*H*$_3$)$_2$), 1.05 (d, $^3J_{HH}$ = 6.2 Hz, 24H, CH(C*H*$_3$)$_2$), 0.92 (d, $^3J_{HH}$ = 6.7 Hz, 24H, CH(C*H*$_3$)$_2$), -2.23 (br s, 3H, Ru*H*B), -15.72 (s, 1H, Ru*H*). $^1$H NMR (500 MHz, $C_6H_5F$, 298 K): δ 8.37 (s, 8H, *o*-Ar*H*), 7.68 (s, 4H, *p*-Ar*H*), 2.81 (br s, 4H, C*H*($CH_3$)$_2$), 2.68 (s, 1H, N*H*), 2.53 (br s, 4H, C*H*($CH_3$)$_2$), 1.86 (s, 6H, N(C*H*$_3$)$_2$), 1.04 (d, $^3J_{HH}$ = 5.8 Hz, 12H, CH(C*H*$_3$)$_2$), 0.99 (d, $^3J_{HH}$ = 6.6 Hz, 12H, CH(C*H*$_3$)$_2$), 0.95 (br s, 12H, CH(C*H*$_3$)$_2$), 0.89 (d, $^3J_{HH}$ = 6.6 Hz, 12H, CH(C*H*$_3$)$_2$), -2.26 (br s, 3H, Ru*H*B), -15.61 (s, 1H, Ru*H*). Selected low temperature $^1$H{$^{11}$B} NMR (400 MHz, $CD_2Cl_2$, 190 K): δ -3.94 (s, 1H, Ru*H*B), -5.83 (s, 1H, Ru*H*B), -15.33 (s, 1H, Ru*H*). $^{11}$B NMR (161 MHz, $C_6H_5F$, 298 K): δ 4.5 (br s, RuH*B*). IR (KBr, cm$^{-1}$): 1991 ($\nu_{RuH}$), 1953 ($\nu_{CO}$). Anal. Calcd for $C_{89}H_{95}B_2N_5OF_{24}Ru$: C 58.42, H 5.23, N 3.83. Found: C 58.35, H 5.02, N 3.87.

**[Ru(IPr)$_2$(CO)(κ$^2$-H$_2$BH·NH$_3$)H]BAr$^F_4$ (6).** $H_3B{\cdot}NH_3$ (0.0004 g, 0.01 mmol) was added to solution of **2** (0.021 g, 0.01 mmol) in $C_6H_5F$ (0.5 mL). After 2 h, the solvent was removed in vacuo, the residue washed with hexane (3 x 0.4 mL) and dried under vacuum. Recrystallization from fluorobenzene/hexane gave pale yellow crystals of **6**. Yield: 0.013 g (61 %). $^1$H NMR (500 MHz, $CD_2Cl_2$, 298 K): δ 7.73 (s, 8H, *o*-Ar*H*), 7.57 (s, 4H, *p*-Ar*H*), 7.46 (t, $^3J_{HH}$ = 7.7 Hz, 4H, Ar*H*), 7.20 (d, $^3J_{HH}$ = 7.8 Hz, 4H, Ar*H*), 7.18 (d, $^3J_{HH}$ = 8.0 Hz, 4H, Ar*H*), 6.99 (s, 4H, NC*H*), 2.89 (br s, 3H, N*H*$_3$), 2.56 (sept, $^3J_{HH}$ = 6.6 Hz, 4H, C*H*($CH_3$)$_2$), 2.47 (sept, $^3J_{HH}$ = 7.0 Hz, 4H, C*H*($CH_3$)$_2$), 1.03 (d, $^3J_{HH}$ = 7.0 Hz, 12H, CH(C*H*$_3$)$_2$), 1.00 (d, $^3J_{HH}$ = 6.6 Hz, 12H, CH(C*H*$_3$)$_2$), 0.93 (d, $^3J_{HH}$ = 7.0 Hz, 12H, CH(C*H*$_3$)$_2$), 0.88 (d, $^3J_{HH}$ = 6.6 Hz, 12H, CH(C*H*$_3$)$_2$), -2.15 (br s, 3H, Ru*H*B), -15.86 (s, 1H, Ru*H*). Selected low temperature $^1$H{$^{11}$B} NMR (400 MHz, $CD_2Cl_2$, 190 K): δ -4.13 (s, 1H, Ru*H*B), -5.63 (s, 1H, Ru*H*B), -14.95 (s, Ru*H*). $^1$H NMR (500 MHz, $C_6H_5F$, 298 K): δ 8.36 (s, 8H, *o*-Ar*H*), 7.67 (s, 4H, *p*-Ar*H*), 2.88 (br s, 3H $NH_3$), 2.67 (sept, $^3J_{HH}$ = 6.9 Hz, 4H, C*H*($CH_3$)$_2$), 2.55 (sept, $^3J_{HH}$ = 7.0 Hz, 4H, C*H*($CH_3$)$_2$), 1.03 (d, $^3J_{HH}$ = 6.9 Hz, 12H, CH(C*H*$_3$)$_2$), 0.98 (d, $^3J_{HH}$ = 6.9 Hz, 12H, CH(C*H*$_3$)$_2$), 0.94 (d, $^3J_{HH}$ = 6.9 Hz, 12H, CH(C*H*$_3$)$_2$), 0.90 (d, $^3J_{HH}$ = 6.9 Hz, 12H, CH(C*H*$_3$)$_2$), -2.05 (br s, 3H, Ru*H*B), -15.88 (s, 1H, Ru*H*). $^{11}$B NMR (161 MHz, $CD_2Cl_2$, 298 K): δ -2.4 (br s, RuH*B*). IR (KBr, cm$^{-1}$): 1948 ($\nu_{CO}$). Anal. Calcd for $C_{87}H_{90}N_5B_2N_5OF_{24}Ru{\cdot}C_6H_5F$: 58.90 H 5.10 N 3.69. Found: C 58.35, H 5.02, N 3.87.

**[Ru(IPr)$_2$(CO)(Bcat)]BAr$^F_4$ (8).** HBcat (0.003 g, 0.025 mmol) was added to a solution of **2** (0.041 g, 0.023 mmol) in $C_6H_5F$ (0.5 mL) and the reaction mixture allowed to stand for 1 h. The solvent was removed under vacuum to yield a pale brown solid, which was washed with hexane (3 x 0.8 mL) and then redissolved in fluorobenzene/hexane to afford **8** as pale yellow crystals Yield: 0.034 g (78%). $^1$H NMR (500 MHz, $CD_2Cl_2$, 298 K): δ 7.73 (s, 8H, *o*-Ar*H*), 7.57 (s, 4H, *p*-Ar*H*), 7.27 (m, 4H, Ar*H*), 7.21 (m, 4H, Ar*H*), 7.02 (d, $^3J_{HH}$ = 7.4 Hz, 4H, Ar*H*), 6.97 (s, 4H, NC*H*), 6.72 (dd, $^3J_{HH}$ = 5.4 Hz, $^3J_{HH}$ = 3.6 Hz, 2H, Ar*H*), 6.35 (dd, $^3J_{HH}$ = 5.4 Hz, $^3J_{HH}$ = 3.6 Hz, Ar*H*), 2.48 (sept, $^3J_{HH}$ = 6.8 Hz, 4H, C*H*($CH_3$)$_2$), 2.31 (sept, $^3J_{HH}$ = 6.8 Hz, 4H, C*H*($CH_3$)$_2$), 1.06 (d, $^3J_{HH}$ = 6.8 Hz, 24H, C*H*($CH_3$)$_2$), 0.88 (d, $^3J_{HH}$ = 6.8 Hz, 12H, CH(C*H*$_3$)$_2$), 0.75 (d, $^3J_{HH}$ = 6.8 Hz, 12H, CH(C*H*$_3$)$_2$). Selected low temperature $^1$H NMR (400 MHz, $CD_2Cl_2$, 182 K): δ 2.70 (sept, $^3J_{HH}$ = 5.1 Hz, 1H, C*H*($CH_3$)$_2$), 2.50 (sept, $^3J_{HH}$ = 6.7 Hz, 1H, C*H*($CH_3$)$_2$), 2.42 (sept, $^3J_{HH}$ = 6.2 Hz, 1H, C*H*($CH_3$)$_2$), 2.35 (sept, $^3J_{HH}$ = 6.0 Hz, 1H, C*H*($CH_3$)$_2$), 2.23 (m, 1H, C*H*($CH_3$)$_2$), 2.13 (sept, $^3J_{HH}$ = 5.7 Hz, 1H, C*H*($CH_3$)$_2$), 1.97 (sept, $^3J_{HH}$ = 5.8 Hz, 1H, C*H*($CH_3$)$_2$), 1.68 (sept, $^3J_{HH}$ = 6.5 Hz, 1H, C*H*($CH_3$)$_2$), 1.38 (br s, 3H, CH(C*H*$_3$)$_2$), 1.26 (br s, 6H, CH(C*H*$_3$)$_2$), 1.20 (br s, 3H, CH(C*H*$_3$)$_2$), 1.15 (br s, 3H, CH(C*H*$_3$)$_2$), 1.10 (br s, 3H, CH(C*H*$_3$)$_2$), 0.97 (br s, 3H, CH(C*H*$_3$)$_2$), 0.88 (br s, 3H, CH(C*H*$_3$)$_2$), 0.81 (d, $^3J_{HH}$ = 6.0 Hz, 3H, CH(C*H*$_3$)$_2$), 0.76 (d, $^3J_{HH}$ = 5.1 Hz, 6H, CH(C*H*$_3$)$_2$), 0.62 (d, $^3J_{HH}$ = 5.7 Hz, 3H, CH(C*H*$_3$)$_2$), 0.49 (d, $^3J_{HH}$ = 6.5 Hz, 3H, CH(C*H*$_3$)$_2$), 0.32 (br s, 6H, CH(C*H*$_3$)$_2$), -0.34 (d, $^3J_{HH}$ = 6.0 Hz, 3H, CH(C*H*$_3$)$_2$). $^{13}$C{$^1$H} NMR (101 MHz, $CD_2Cl_2$, 298 K): δ 199.4 (s, Ru-*C*O), 182.2 (s, Ru-$C_{NHC}$), 162.2 (q, $^1J_{CB}$ = 50 Hz, *i*-Ar*C*), 149.5 (s, O*C*), 145.2 (s, *o*-Ar*C*), 135.3 (s, NAr*C*), 135.2 (s, *o*-Ar*C*), 130.8 (s, *p*-Ar*C*), 129.0 (qq, $^2J_{CF}$ = 32 Hz, $^4J_{CF}$ = 3 Hz, *m*-Ar*C*), 126.9 (s, NCH),125.8 (s, *m*-Ar*C*), 125.0 (q, $^1J_{CF}$ = 271 Hz, *C*F$_3$), 124.6 (s, *m*-Ar*C*), 120.9 (s, Ar*C*), 117.8 (sept, $^3J_{CF}$ = 4 Hz, *p*-Ar*C*), 112.1 (s, Ar*C*), 29.8 (s, *C*H($CH_3$)$_2$), 29.1 (s, *C*H($CH_3$)$_2$), 25.1 (s, CH(*C*H$_3$)$_2$), 24.8 (s, CH(*C*H$_3$)$_2$), 22.4 (s, CH(*C*H$_3$)$_2$), 21.2 (s, CH(*C*H$_3$)$_2$). $^{11}$B NMR (161 MHz, $CD_2Cl_2$ 298 K): δ 41.6 (br s, Ru*B*). IR ($CD_2Cl_2$, cm$^{-1}$): 1981 ($\nu_{CO}$). Anal. Calcd for $C_{93}H_{88}B_2N_4O_3F_{24}Ru$: C 59.14, H 4.70, N 2.97. Found: C 59.01, H 4.55, N 3.08.

**Catalytic Hydroboration.** To a solution of **2** (0.004 g, 0.0022 mmol) in $C_6H_5F$ (0.5 mL) in a vial in the glovebox was added 1-hexene (0.004 g, 0.0440 mmol) and HBcat (0.011 g, 0.088 mmol) and the reaction mixture stirred for 24 h. At this time, $^1$H NMR spectroscopy showed no resonances attributable to any remaining 1-hexene. The composition of the reaction mixture was analyzed by GC-MS; assignment of the linear product (and, by default, therefore the branched product) was made by comparison of retention time to a sample comprising ca. 99% of linear isomer prepared via the hydroboration of 1-hexene using $Rh(PPh_3)_3Cl$.[51]

**Crystallography.** Data for the combined X-ray (Mo-Kα) and neutron refinement of **2** were collected using a Nonius kappaCCD diffractometer and on the SXD time-of-flight Laue single crystal diffractometer instrument at the ISIS spallation neutron source,[52] respectively. The neutron experiment for **2** was carried out using two single crystals that were mounted in random orientations relative to each other inside a sealed vanadium container filled with argon gas.[53] The vanadium can was loaded into a top-loading closed cycle refrigerator and data collected at 3 different orientations. A Nonius kappaCCD was also employed for the data collection of **3**, while those for **5** and **6** were effected using an Agilent Xcalibur (Mo-*K*α) diffractometer and that for **7** was completed using an Agilent SuperNova (Cu-*K*α) diffractometer. The structure of **8** was refined using a combination of X-ray data garnered using Cu-*K*α radiation and an Agilent SuperNova diffractometer plus neutron data on the SXD instrument at ISIS. In the latter experiment, one crystal was sealed inside a vanadium container under argon and placed into a top loading closed cycle refrigerator with data collected at 5 different orientations. All diffraction measurements were made at 150 K.

All of the X-ray refinements were carried out using SHELXL.[54] With the exception of **6**, the asymmetric unit in all structures comprizes one cation and one $BAr_4^F$ anion. Hydrides, where present, were located and refined at a distance of 1.6 Å from the metal center in the case of the X-ray-only refinements for **3**, **5** and **6**. Disorder of the fluorine atoms in some of the anion $CF_3$ groups was not uncommon. In such instances, C-F and F···F distance restraints were included and, if merited, ADP restraints were added for affected fractional occupancy fluorine atoms. Convergence was reasonably straightforward with the exception of the pertinent details, many of which pertain to disorder, that follow.

The model in **2** was solved and refined using X-ray data, where two of the isopropyl groups in the cation revealed disorder, with the positions of C54/C55 and the carbon atoms attached to C41 (C42/C43) each being split over 2 sites in a 55:45 ratio. Some C-C distance restraints were employed to help convergence to a chemically sensible finale. The hydrogen atoms attached to C51 were located and freely refined, subject to being located 0.98 Å from the parent atom. The hydride ligand was seen to be disordered over two *trans* sites (55:45 ratio) and each fraction was refined at a distance of 1.6 Å from Ru1. In the $BAr_4^F$ anion, the fluorines attached to C79, C86 and C87 each exhibited disorder over two sites in respective ratios of 70:30, 60:40 and 50:50. The arising converged X-ray model was used as the basis for the results presented here, which were obtained using Jana2006[55] and a combination of X-ray and neutron data. With the exception of H51A, H51B and H51C, and the disordered hydride (H1/H1A) hydrogens were initially refined in four groups, namely, those confined to the anion and, in the cation, primary hydrogens, tertiary hydrogens and aromatic hydrogens. The arising refined C-H distances were used as the basis for the rigid groups with which these non-contentious hydrogens were ultimately included. The disordered hydride was modelled subject to both components being equidistant from the ruthenium center. The agostic hydrogens attached to C51 were refined freely. All hydrogen atoms were treated isotropically. Disordered fluorine atoms were refined with ADP restraints, and with restrained C-F and F...F distances of 1.330(5) Å and 2.135(30) Å, respectively.

Halide disorder was seen to bedevil many of the $CF_3$ groups in the anion in **3**. In particular, the fluorine atoms attached to C64, C65 C72 C80, C81 and C89 exhibited respective disorders of 65:35, 50:50. 70:30, 50:50, 80:20 and 55:45. C-F distances were restrained to being similar within each affected functionality. The isopropyl carbons, C23/C24, belonging to the cation in **6** were modelled as being disordered over two sites in a 55:45 ratio. The hydrogen atom attached to C22 was included at a calculated position based on the major fractional occupancy components of C23/C24. H5 (attached to N5) was located and refined subject to being located at a distance of 0.98 Å from the parent atom. The hydrogen atoms attached to the boron center, B1, were located and refined without restraints. Disorder was also evident in some of the anion $CF_3$ groups. In particular, the fluorine atoms attached to C64, C72 and C73 were each modelled over two proximate sites in disorder ratios of 50:50, 60:40, and 60:40, respectively. In **6,** the hydrogen atoms attached to B1 and N5 were readily located and freely refined, without any restraints. There may be some "wagging" disorder associated with the carbonyl ligand. However, efforts to model this did not improve the refinement; hence, these were abandoned. Only one $CF_3$ group in the anion was modelled for disorder, with the fluorines attached to C62 being treated as located across two sites in a 75:25 ratio. There was also one disordered molecule of fluorobenzene in the asymmetric unit of this structure. This was ultimately treated using PLATON SQUEEZE, as the solvent was disordered over two proximate sites and, in each of these, the fractional fluorine was additionally disordered.

The asymmetric unit in **7** comprizes one cation, one anion, half of an ordered molecule of $C_6H_5F$ and a region of diffuse solvent. C88, C91, H91 and F26 in the ordered solvent moiety are coincident with a crystallographic 2-fold rotation axis which serves to generate the remainder of the molecule. The disordered region exhibited some evidence for the presence of one fluorobenzene molecule, but this was not accessible to any sensible model and hence was treated via PLATON SQUEEZE. On the basis of the results from this algorithm, the empirical formula (as presented herein) contains one additional formula unit of $C_6H_5F$, to account for the SQUEEZED solvent. The hydrogen atoms attached to C51 were located and refined at a distance of 0.98 Å from the parent atom and subject to being equidistant from each other. In the anion, F16-18 were refined as being disordered over two proximate sites in a 65:35 ratio.

As for **2**, the structure of **8** was solved to convergence using X-ray data and the arising model then used as the basis for a combined refinement[55] using both X-ray and neutron data. In the X-ray only model, the hydrogens attached to C27 were located and refined at a distance of 0.98 Å from the parent atom and with a common $U_{iso}$ value. Additionally, the hydrogen atoms attached to C12 were included at calculated positions but, again, with a common $U_{iso}$. Two of the $CF_3$ groups in the anion were modelled for disorder (55:45 and 60:40 ratios for fluorine atoms attached to C69 and C76, respectively). The combined X-ray and neutron refinement for this structure, with particular emphasis on the treatment of non-contentious hydrogen atoms, was similar to the strategy adopted for **2**. Ultimately, in this instance, the hydrogens attached to C27 were refined without restraints.

Crystallographic data for compounds **2**, **3**, and **5-8** have been deposited with the Cambridge Crystallographic Data Centre as supplementary publication CCDC 1435594-1435599. Copies of the data can be obtained free of charge on application to CCDC, 12 Union Road, Cambridge CB2 1EZ, UK [fax(+44) 1223 336033, e-mail: deposit@ccdc.cam.ac.uk].

**Computational Details.** DFT calculations were run with Gaussian 03 (Revision D.01)[56] and Gaussian 09 (Revision D.01).[57] Ru centers were described with the Stuttgart RECPs and associated basis sets[58] and 6-31G** basis sets were used for all other atoms.[59] Optimizations employed the BP86[60] functional and all stationary points were fully characterized via analytical frequency calculations as either minima (all positive eigenvalues) or transition states (one negative eigenvalue). Exceptions were those structures used for the QTAIM and NBO studies which were either based on the X-ray/neutron structures (**2a**, **2b**, **8**) or the experimental heavy atom positions with only the H atoms positions being optimized (**7**). **TS(4b-4b)** was also characterized via IRC calculations and subsequent geometry optimizations to confirm it linked to the expected minima. PCM corrections for the effects of fluorobenzene and $CH_2Cl_2$ solvent were computed as appropriate with Gaussian 09 and dispersion corrections applied using Grimme's D3 parameter set[61] using the BP86-optimised geometries. QTAIM studies employed the AIMALL program[62] and NBO analyses were run with NBO version 5.9.[63]

## ASSOCIATED CONTENT

### Supporting Information

The Supporting Information is available free of charge on the ACS Publications website. Multinuclear NMR spectra of **2-6** and **8**. Computational Data including full QTAIM data for BCPs and RCPs associated with Ru···H agostic interactions, details of TDDFT calculations, optimized geometries and energies and geometries used in QTAIM calculations and an NBO analysis of the agostic interactions in **2a**, **2b** and **8**; an xyz file containing all geometries is also supplied.

## AUTHOR INFORMATION


### Corresponding Author

* E-mail: m.k.whittlesey@bath.ac.uk. Tel.: 44 1225 383748

### Present Address

[δ] School of Chemistry, University of St Andrews, St Andrews, Fife KY16 9ST, UK.


### Notes

The authors declare no competing financial interest.

## ACKNOWLEDGMENT


We acknowledge the experimental assistance of Drs John Lowe (NMR), Matthew Jones (GC-MS) and Mark Hutchby (GC). Prof Vaclav Petricek is thanked for useful discussions on the Jana refinements. Experiments at the ISIS Pulsed Neutron and Muon Source were supported by a beamtime allocation (Experiment 1510181) from the Science and Technology Facilities Council (STFC). The EPSRC (grants EP/J009962/1 and EP/J010677/1) are thanked for financial support.


## REFERENCES


(1) Chatt, J.; Davidson, J. M. *J. Chem. Soc.* **1965**, 843-855.

(2) (a) Ittel, S. D.; Tolman, C. A.; English, A. D.; Jesson, J. P. *J. Am. Chem. Soc.* **1976**, *98*, 6073-6075. (b) Ittel, S. D.; Tolman, C. A.; English, A. D.; Jesson, J. P. *J. Am. Chem. Soc.* **1978**, *100*, 7577-7585. (c) Tolman, C. A.; Ittel, S. D.; English, A. D.; Jesson, J. P. *J. Am. Chem. Soc.* **1979**, *101*, 1742-1751.

(3) (a) Hall, C.; Jones, W. D.; Mawby, R. J.; Osman, R.; Perutz, R. N.; Whittlesey, M. K. *J. Am. Chem. Soc.* **1992**, *114*, 7425-7435. (b) Osman, R.; Perutz, R. N.; Rooney, A. D.; Langley, A. J. *J. Phys. Chem.* **1994**, *98*, 3562-3563.

(4) (a) Ogasawara, M.; Macgregor, S. A.; Streib, W. E.; Folting, K.; Eisenstein, O.; Caulton, K. G. *J. Am. Chem. Soc.* **1995**, *117*, 8869-8870. (b) Ogasawara, M.; Macgregor, S. A.; Streib, W. E.; Folting, K.; Eisenstein, O.; Caulton, K. G. *J. Am. Chem. Soc.* **1996**, *118*, 10189-10199. See also: Ogasawara, M.; Huang, D.; Streib, W. E.; Huffman, J. C.; Gallego-Planas, N.; Maseras, F.; Eisenstein, O.; Caulton, K. G. *J. Am. Chem. Soc.* **1997**, *119*, 8642-8651.

(5) Flügel, R.; Windmüller, B.; Gevert, O.; Werner, H. *Chem. Ber.* **1996**, *129*, 1007-1013.

(6) (a) Watson, L. A.; Ozerov, O. V.; Pink, M.; Caulton, K. G. *J. Am. Chem. Soc.* **2003**, *125*, 8426-8427. (b) Ingleson, M. J.; Yang, X.; Pink, M.; Caulton, K. G. *J. Am. Chem. Soc.* **2005**, *127*, 10846-10847. (c) Walstrom, A.; Pink, M.; Caulton, K. G. *Inorg. Chem.* **2006**, *45*, 5617-5620.

(7) (a) Askevold, B.; Khusniyarov, M. M.; Herdtweck, E.; Meyer, K.; Schneider, S. *Angew. Chem. Int. Ed.* **2010**, *49*, 7566-7569. (b) Schneider, S.; Meiners, J.; Askevold, B. *Eur. J. Inorg. Chem.* **2012**, 412-429. (c) Askevold, B.; Khusniyarov, M. M.; Kroener, W.; Gieb, K.; Müller, P.; Herdtweck, E.; Heinemann, M.; Diefenbach, M.; Holthausen, M. C.; Vieru, V.; Chibotaru, L. F.; Schneider, S. *Chem. Eur. J.* **2015**, *21*, 579-589.

(8) MacInnis, M. C.; McDonald, R.; Ferguson, M. J.; Tobisch, S.; Turculet, L. *J. Am. Chem. Soc.* **2011**, *133*, 13622-13633.

(9) Huang, D.; Streib, W. E.; Eisenstein, O.; Caulton, K. G. *Angew. Chem. Int. Ed. Engl.* **1997**, *36*, 2004-2006.

(10) Huang, D.; Streib, W. E.; Bollinger, J. C.; Caulton, K. G.; Winter, R. F.; Scheiring, T. *J. Am. Chem. Soc.* **1999**, *121*, 8087-8097.

(11) Huang, D.; Bollinger, J. C.; Streib, W. E.; Folting, K.; Young, V., Jr.; Eisenstein, O.; Caulton, K. G. *Organometallics* **2000**, *19*, 2281-2290.

(12) Baratta, W.; Herdtweck, E.; Rigo, P. *Angew. Chem. Int. Ed.* **1999**, *38*, 1629-1631.

(13) (a) Huang, D.; Folting, K.; Caulton, K. G. *J. Am. Chem. Soc.* **1999**, *121*, 10318-10322. (b) Huang, D.; Gérard, H.; Clot, E.; Young, V., Jr.; Streib, W. E.; Eisenstein, O.; Caulton, K. G. *Organometallics* **1999**, *18*, 5441-5443.

(14) Catalá, R.-M.; Cruz-Garritz, D.; Sosa, P.; Terreros, P.; Torrens, H.; Hills, A.; Hughes, D. L.; Richards, R. L. *J. Organomet. Chem.* **1989**, *359*, 219-232.

(15) For cases which seem to be devoid of such stabilization, see: (a) Sanford, M. S.; Henling, L. M.; Day, M. W.; Grubbs, R. H. *Angew. Chem. Int. Ed.* **2000**, *39*, 3451-3453. (b) Conrad, J. C.; Amoroso, D.; Czechura, P.; Yap, G. P. A.; Fogg, D. E. *Organometallics* **2003**, *22*, 3634-3636. (c) Romero, P. E.; Piers, W. E.; McDonald, R. *Angew. Chem. Int. Ed.* **2004**, *43*, 6161-6165. (d) Singh, A. K.; Levine, B. G.; Staples, R. J.; Odom, A. L. *Chem. Commun.* **2013**, *49*, 10799-10801.

(16) Baratta, W.; Mealli, C.; Herdtweck, E.; Ienco, A.; Mason, S. A.; Rigo, P. *J. Am. Chem. Soc.* **2004**, *126*, 5549-5562. For other non Ru examples, see: (a) Crosby, S. H.; Clarkson, G. J.; Rourke, J. P. *J. Am. Chem. Soc.* **2009**, *131*, 14142-14143. (b) Cole, J. M.; Waddell, P. G.; Wheatley, A. E. H.; McIntyre, G. J.; Peel, A. J.; Tate, C. W.; Linton, D. J. *Organometallics* **2014**, *33*, 3919-3923.

(17) Lee, J. P.; Ke, Z.; Ramírez, M. A.; Gunnoe, T. B.; Cundari, T. R.; Boyle, P. D.; Petersen, J. L. *Organometallics* **2009**, *28*, 1758-1775.

(18) (a) Scott, N. M.; Dorta, R.; Stevens, E. D.; Correa, A.; Cavallo, L.; Nolan, S. P. *J. Am. Chem. Soc.* **2005**, *127*, 3516-3526. (b) Fantasia, S.; Egbert, J. D.; Jurčík, V.; Cazin, C. S. J.; Jacobsen, H.; Cavallo, L.; Heinekey, D. M.; Nolan, S. P. *Angew. Chem. Int. Ed.* **2009**, *48*, 5182-5186.

(19) Chantler, V. L.; Chatwin, S. L.; Jazzar, R. F. R.; Mahon, M. F.; Saker, O.; Whittlesey, M. K. *Dalton Trans.* **2008**, 2603-2614.

(20) (a) Rivada-Wheelaghan, O.; Donnadieu, B.; Maya, C.; Conejero, S., *Chem. Eur. J.* **2010**, *16*, 10323-10326. (b) Ortuño, M. A.; Conejero, S.; Lledós, A., *Beilstein J. Org. Chem.* **2013**, *9*, 1352-1382.

(21) *Atoms in Molecules - A Quantum Theory* R.F.W. Bader, Oxford University Press, Oxford, **1990**.

(22) Batool, M.; Martin, T. A.; Algarra, A.; George, M. W.; Macgregor, S. A.; Mahon, M. F.; Whittlesey, M. K. *Organometallics* **2012**, *31*, 4971-4979.

(23) See ESI for figure showing the minor component.

(24) For recent discussions on the dynamics of agostically bound NHC ligands in low-coordinate cationic Pt(II) species, see: (a) Ortuño, M. A.; Vidossich, P.; Ujaque, G.; Conejero, S.; Lledós, A. *Dalton Trans.* **2013**, *42*, 12165-12172. (b) Ortuño, M. A.; Vidossich, P.; Conejero, S.; Lledós, A. *Angew. Chem. Int. Ed.* **2014**, *53*, 14158-14161.

(25) Huang, D.; Huffman, J. C.; Bollinger, J. C.; Eisenstein, O.; Caulton, K. G. *J. Am. Chem. Soc.* **1997**, *119*, 7398-7399.

(26) Tang, C. Y.; Thompson, A. L.; Aldridge, S. *J. Am. Chem. Soc.* **2010**, *132*, 10578-10591.

(27) As Gunnoe, Cundari and co-workers employed the B3LYP functional in their work[17] we repeated our calculations with the B3LYP-D3($C_6H_5F$)//B3LYP approach. This gave similar trends to the results in the main text, for $[Ru(IPr)_2(CO)(H)]^+$ (**2b** (0.0 kcal/mol) < **2a** (+0.3 kcal/mol) < **2c** (+3.3 kcal/mol)) and for $[Ru(IMes)_2(CO)(H)]^+$ (**1c** (0.0 kcal/mol) < **1a** (+1.4 kcal/mol) < **1b** (+7.5 kcal/mol)). See ESI for full details.

(28) Siedle, A. R.; Newmark, R. A.; Gleason, W. B. *Inorg. Chem.* **1991**, *30*, 2005-2009.

(29) (a) Gusev, D. G.; Hübener, R.; Burger, P.; Orama, O.; Berke, H. *J. Am. Chem. Soc.* **1997**, *119*, 3716-3731. (b) Chen, Y.-Z.; Chan, W. C.; Lau, C. P.; Chu, H. S.; Lee, H. L.; Jia, G. *Organometallics* **1997**, *16*, 1241-1246. (c) Leñero, K. A.; Kranenburg, M.; Guari, Y.; Kamer, P. C. J.; van Leeuwen, P. W. N. M.; Sabo-Etienne, S.; Chaudret, B. *Inorg. Chem.* **2003**, *42*, 2859-2866. (d) Grellier, M.; Vendier, L.; Chaudret, B.; Albinati, A.; Rizzato, S.; Mason, S.; Sabo-Etienne, S. *J. Am. Chem. Soc.* **2005**, *127*, 17592-17593.

(30) For a review of $M(\eta^2\text{-}H_2)H$ species, see: Morris, R. H. *Coord. Chem. Rev.* **2008**, *252*, 2381-2394.

(31) This contrasts markedly to one of the few other known Ru-NHC dihydrogen complexes, $[Ru(NHC)_4(\eta^2\text{-}H_2)H]BAr_4^F$, which for both of the small N-alkyl substituted NHCs 1,3-diethyl-4,5-dimethylimidazol-2-ylidene ($IEt_2Me_2$) and 1,2,4,5-tetramethylimidazol-2-ylidene ($IMe_4$), readily lose $H_2$ upon freeze-pump-thaw degassing. Burling, S.; Häller, L. J. L.; Mas-Marzá, E.; Moreno, A.; Macgregor, S. A.; Mahon, M. F.; Pregosin, P. S.; Whittlesey, M. K. *Chem. Eur. J.* **2009**, *15*, 10912-10923.

(32) Alcaraz, G.; Sabo-Etienne, S. *Angew. Chem. Int. Ed.* **2010**, *49*, 7170-7179.

(33) Douglas, T. M.; Chaplin, A. B.; Weller, A. S. *J. Am. Chem. Soc.* **2008**, *130*, 14432-14433.

(34) Jaska, C. A.; Temple, K.; Lough, A. J.; Manners, I. *J. Am. Chem. Soc.* **2003**, *125*, 9424-9434.

(35) Douglas, T. M.; Chaplin, A. B.; Weller, A. S.; Yang, X.; Hall, M. B. *J. Am. Chem. Soc.* **2009**, *131*, 15440-15456.

(36) Tang, C. Y.; Thompson, A. L.; Aldridge, S. *Angew. Chem. Int. Ed.* **2010**, *49*, 921-925.

(37) Ledger, A. E. W.; Ellul, C. E.; Mahon, M. F.; Williams, J. M. J.; Whittlesey, M. K. *Chem. Eur. J.* **2011**, *17*, 8704-8713.

(38) Kawano, Y.; Hashiva, M.; Shimoi, M. *Organometallics* **2006**, *25*, 4420-4426.

(39) Stevens, C. J.; Dallanegra, R.; Chaplin, A. B.; Weller, A. S.; Macgregor, S. A.; Ward, B.; McKay, D.; Alcaraz, G.; Sabo-Etienne, S. *Chem. Eur. J.* **2011**, *17*, 3011-3020.

(40) Alcaraz, G.; Vendier, L.; Clot, E.; Sabo-Etienne, S. *Angew. Chem. Int. Ed.* **2010**, *49*, 918-920.

(41) Alcaraz, G.; Chaplin, A. B.; Stevens, C. J.; Clot, E.; Vendier, L.; Weller, A. S.; Sabo-Etienne, S. *Organometallics* **2010**, *29*, 5591-5595.

(42) (a) Sewell, L. J.; Chaplin, A. B.; Weller, A. S. *Dalton Trans.* **2011**, *40*, 7499-7501. (b) Johnson, H. C.; Torry-Harris, R.; Ortega, L.; Theron, R.; McIndoe, J. S.; Weller, A. S. *Catal. Sci. Technol.* **2014**, *4*, 3486-3494.

(43) Tang, C. Y.; Smith, W.; Vidovic, D.; Thompson, A. L.; Chaplin, A. B.; Aldridge, S. *Organometallics* **2009**, *28*, 3059-3066.

(44) (a) Lu, Z.; Jun, C.-H.; de Gala, S. R.; Sigalas, M. P.; Eisenstein, O.; Crabtree, R. H. *Organometallics* **1995**, *14*, 1168-1175. (b) Rickard, C. E. F.; Roper, W. R.; Williamson, A.; Wright, L. J. *Organometallics* **1998**, *17*, 4869-4874. (c) Braunschweig, H.; Radacki, K.; Rais, D.; Scheschkewitz, D. *Angew. Chem. Int. Ed.* **2005**, *44*, 5651-5654. (d) Braunschweig, H.; Radacki, K.; Uttinger, K. *Chem. Eur. J.* **2008**, *14*, 7858-7866. (e) Arnold, N.; Braunschweig, H.; Brenner, P.; Jimenez-Halla, J. O. C.; Kupfer, T.; Radacki, K. *Organometallics* **2012**, *31*, 1897-1907. (f) Buil, M. L.; Esteruelas, M. A.; Fernández, I.; Izquierdo, S.; Õnate, E. *Organometallics* **2013**, *32*, 2744-2752.

(45) (a) Irvine, G. J.; Lesley, M. J. G.; Marder, T. B.; Norman, N. C.; Rice, C. R.; Robins, E. G.; Roper, W. R.; Whittell, G. R.; Wright, L. J. *Chem. Rev.* **1998**, *98*, 2685-2722. (b) Kays, D. L.; Aldridge, S. *Struct. Bond.* **2008**, *130*, 29-122. (c) Aldridge, S.; Coombs, D. L. *Coord. Chem. Rev.* **2004**, *248*, 535-559.

(46) (a) Lam, K. C.; Lam, W. H.; Lin, Z.; Marder, T. B.; Norman, N. C. *Inorg. Chem.* **2004**, *43*, 2541-2547. (b) Zhu, J.; Lin, Z. Y.; Marder, T. B. *Inorg. Chem.* **2005**, *44*, 9384-9390.

(47) Dang, L.; Lin, Z.; Marder, T. B. *Chem. Commun.* **2009**, 3987-3995.

(48) (a) Rickard, C. E. F.; Roper, W. R.; Williamson, A.; Wright, L. J. *Organometallics* **2000**, *19*, 4344-4355. (b) Clark, G. R.; Irvine, G. J.; Roper, W. R.; Wright, L. J. *J. Organomet. Chem.* **2003**, *680*, 81-88. (c) Rickard, C. E. F.; Roper, W. R.; Williamson, A.; Wright, L. J. *J. Organomet. Chem.* **2004**, *689*, 1609-1616. (d) Rankin, M. A.; MacLean, D. F.; McDonald, R.; Ferguson, M. J.; Lumsden, M. D.; Stradiotto, M. *Organometallics* **2009**, *28*, 74-83. (e) Hill, A. F.; Lee, S. B.; Park, J.; Shang, R.; Willis, A. C. *Organometallics* **2010**, *29*, 5661-5669. (f) Koren-Selfridge, L.; Query, I. P.; Hanson, J. A.; Isley, N. A.; Guzei, I. A.; Clark, T. B. *Organometallics* **2010**, *29*, 3896-3900. (g) Hill, A. F.; McQueen, C. M. A. *Organometallics* **2014**, *33*, 1977-1985.

(49) Beletskaya, I.; Pelter, A. *Tetrahedron* **1997**, *53*, 4957-5026.

(50) (a) Burgess, K.; Jaspars, M. *Organometallics* **1993**, *12*, 4197-4200. (b) Caballero, A.; Sabo-Etienne, S. *Organometallics* **2007**, *26*, 1191-1195.

(51) Evans, D. A.; Fu, G. C.; Hoveyda, A. H. *J. Am. Chem. Soc.* **1992**, *114*, 6671-6679.

(52) Keen, D. A.; Gutmann, M. J.; Wilson, C. C. *J. Appl. Cryst.* **2006**, *39*, 714-722.

(53) Wilson, C. C. *J. Appl. Cryst.* **1997**, *30*, 184-189.

(54) Sheldrick, G. M. *Acta. Crystallogr., Sect A* **1990**, *467-473*, A46. Sheldrick, G. M, SHELXL-97, a computer program for crystal structure refinement, University of Göttingen, 1997.

(55) Petricek, V.; Dusek, M.; Palatinus, L. *Z. Kristallogr.* **2014**, *229*, 345-352.

(56) Frisch, M. J.; Trucks, G. W.; Schlegel, H. B.; Scuseria, G. E.; Robb, M. A.; Cheeseman, J. R.; Montgomery, J. A.; Vreven, T.; Kudin, K. N. B., J. C.; Millam, J. M.; Iyengar, S. S.; Tomasi, J.; Barone, V.; Mennucci, B.; Cossi, M.; Scalmani, G.; Rega, N.; Petersson, G. A.; Nakatsuji, H.; Hada, M.; Ehara, M.; Toyota, K.; Fukuda, R.; Hasegawa, J.; Ishida, M.; Nakajima, T.; Honda, Y.; Kitao, O.; Nakai, H.; Klene, M.; Li, X.; Knox, J. E.; Hratchian, H. P.; Cross, J. B.; Bakken, V.; Adamo, C.; Jaramillo, J.; Gomperts, R.; Stratmann, R. E.; Yazyev, O.; Austin, A. J.; Cammi, R.; Pomelli, C.; Ochterski, J. W.; Ayala, P. Y.; Morokuma, K.; Voth, G. A.;

Salvador, P.; Dannenberg, J. J.; Zakrzewski, V. G.; Dapprich, S.; Daniels, A. D.; Strain, M. C.; Farkas, O.; Malick, D. K.; Rabuck, A. D.; Raghavachari, K.; Foresman, J. B.; Ortiz, J. V.; Cui, Q.; Baboul, A. G.; Clifford, S.; Cioslowski, J.; Stefanov, B. B.; G. Liu, A. L.; Piskorz, P.; Komaromi, I.; Martin, R. L.; Fox, D. J.; Keith, T.; Al-Laham, M. A.; Peng, C. Y.; Nanayakkara, A.; Challacombe, M.; Gill, P. M. W.; Johnson, B.; Chen, W.; Wong, M. W.; Gonzalez, C.; Pople, J. A. Gaussian 03, Revision D.01, Gaussian, Inc.: Wallingford CT, 2004.

(57) Frisch, M. J. T., G. W.; Schlegel, H. B.; Scuseria, G. E.; Robb, M. A.; Cheeseman, J. R.; Scalmani, G.; Barone, V.; Mennucci, B.; Petersson, G. A.; Nakatsuji, H.; Caricato, M.; Li, X.; Hratchian, H. P.; Izmaylov, A. F.; Bloino, J.; Zheng, G.; Sonnenberg, J. L.; Hada, M.; Ehara, M.; Toyota, K.; Fukuda, R.; Hasegawa, J.; Ishida, M.; Nakajima, T.; Honda, Y.; Kitao, O.; Nakai, H.; Vreven, T.; J. A. Montgomery, J.; Peralta, J. E.; Ogliaro, F.; Bearpark, M.; Heyd, J. J.; Brothers, E.; Kudin, K. N.; Staroverov, V. N.; Kobayashi, R.; Normand, J.; Raghavachari, K.; Rendell, A.; Burant, J. C.; Iyengar, S. S.; Tomasi, J.; Cossi, M.; Rega, N.; Millam, J. M.; Klene, M.; Knox, J. E.; Cross, J. B.; Bakken, V.; Adamo, C.; Jaramillo, J.; Gomperts, R.; Stratmann, R. E.; Yazyev, O.; Austin, A. J.; Cammi, R.; Pomelli, C.; Ochterski, J. W.; Martin, R. L.; Morokuma, K.; Zakrzewski, V. G.; Voth, G. A.; Salvador, P.; Dannenberg, J. J.; Dapprich, S.; Daniels, A. D.; Farkas, O.; Foresman, J. B.; Ortiz, J. V.; Cioslowski, J.; Fox, D. J. Gaussian 09, Revision D.01, Gaussian, Inc.: Wallingford CT, 2013.

(58) Andrae, D.; Häußermann, U.; Dolg, M.; Stoll, H.; Preuß, H. *Theor. Chim. Acta* **1990**, *77*, 123-141.

(59) (a) Hehre, W. J.; Ditchfield, R.; Pople, J. A. *J. Chem. Phys.* **1972**, *56*, 2257-2261. (b) Hariharan, P. C.; Pople, J. A. *Theor. Chim. Acta* **1973**, *28*, 213-222.

(60) (a) Perdew, J. P. *Phys. Rev. B* **1986**, *33*, 8822-8824. (b) Becke, A. D. *Phys. Rev. A* **1988**, *38*, 3098-3100.

(61) Grimme, S.; Antony, J.; Ehrlich, S.; Krieg, H. *J. Chem. Phys.* **2010**, *132*, 154104-1.

(62) AIMAll (Version 13.02.26, Professional), Keith, T. A.; Gristmill, T. K. Software, Overland Park KS, USA, 2015 (aim.tkgristmill.com).

(63) NBO 5.9. Glendening, E. D.; Badenhoop, J. K.; Reed, A. E.; Carpenter, J. E.; Bohmann, J. A.; Morales, C. M.; Weinhold, F., (Theoretical Chemistry Institute, University of Wisconsin, Madison, WI, 2009); http://www.chem.wisc.edu/~nbo5

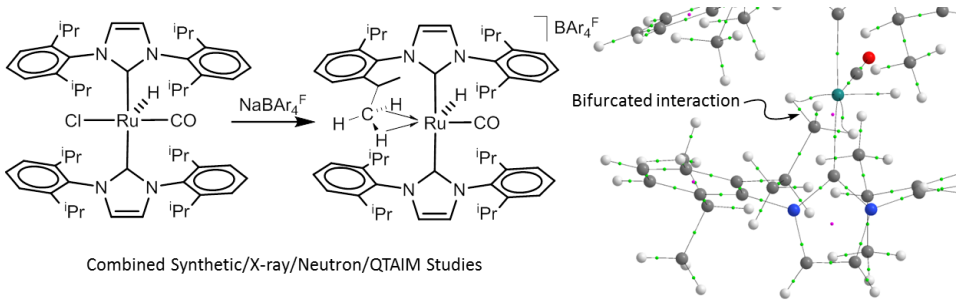


Insert Table of Contents artwork here